core phosphorylated inside the viral particle after release from the infected cells associates directly with Pin1 after entry into host cells for the uncoating process. A better understanding of these findings is crucial not only for elucidating the uncoating process at the early stage of the HIV-1 life cycle but also for identifying new anti-HIV drugs.

Acknowledgments—We thank A. Muneoka (Shin Nippon Biomedical Laboratories, Ltd.) for the technical support during electron microscopy. We thank Dr. R. Swanstrom (Lineberger Comprehensive Cancer Center, University of North Carolina at Chapel Hill) for support in preparing pNL4-3Δenv(S16A/P17A) with the pNL4-3-based env expression vector and helpful discussions.

REFERENCES

1. Goff, S. P. (2001) *J. Gene Med.* **3,** 517–528
2. Dvorin, J. D., and Malim, M. H. (2003) *Curr. Top. Microbiol. Immunol.* **281,** 179–208
3. Auewarakul, P., Wacharapornin, P., Srichatrapimuk, S., Chutipongtanate, S., and Puthavathana, P. (2005) *Virology* **337,** 93–101
4. Warrilow, D., Meredith, L., Davis, A., Burrell, C., Li, P., and Harrich, D. (2008) *J. Virol.* **82,** 1425–1437
5. Zack, J. A., Arrigo, S. J., Weitsman, S. R., Go, A. S., Haislip, A., and Chen, I. S. (1990) *Cell* **61,** 213–222
6. Stevenson, M., Stanwick, T. L., Dempsey, M. P., and Lamonica, C. A. (1990) *EMBO J.* **9,** 1551–1560
7. Misumi, S., Fuchigami, T., Takamune, N., Takahashi, I., Takama, M., and Shoji, S. (2002) *J. Virol.* **76,** 10000–10008
8. Veronese, F. D., Copeland, T. D., Oroszlan, S., Gallo, R. C., and Sarngadharan, M. G. (1988) *J. Virol.* **62,** 795–801
9. Mervis, R. J., Ahmad, N., Lillehoj, E. P., Raum, M. G., Salazar, F. H., Chan, H. W., and Venkatesan, S. (1988) *J. Virol.* **62,** 3993–4002
10. Macaulay, C., Meier, E., and Forbes, D. J. (1995) *J. Biol. Chem.* **270,** 254–262
11. Favreau, C., Worman, H. J., Wozniak, R. W., Frappier, T., and Courvalin, J. C. (1996) *Biochemistry* **35,** 8035–8044
12. Glavy, J. S., Krutchinsky, A. N., Cristea, I. M., Berke, I. C., Boehmer, T., Blobel, G., and Chait, B. T. (2007) *Proc. Natl. Acad. Sci. U.S.A.* **104,** 3811–3816
13. Ott, D. E., Coren, L. V., Kane, B. P., Busch, L. K., Johnson, D. G., Sowder, R. C., 2nd, Chertova, E. N., Arthur, L. O., and Henderson, L. E. (1996) *J. Virol.* **70,** 7734–7743
14. Adachi, A., Gendelman, H. E., Koenig, S., Folks, T., Willey, R., Rabson, A., and Martin, M. A. (1986) *J. Virol.* **59,** 284–291
15. O'Farrell, P. H. (1975) *J. Biol. Chem.* **250,** 4007–4021
16. Kawano, Y., Tanaka, Y., Misawa, N., Tanaka, R., Kira, J. I., Kimura, T., Fukushi, M., Sano, K., Goto, T., Nakai, M., Kobayashi, T., Yamamoto, N., and Koyanagi, Y. (1997) *J. Virol.* **71,** 8456–8466
17. Ikeda, T., Nishitsuji, H., Zhou, X., Nara, N., Ohashi, T., Kannagi, M., and Masuda, T. (2004) *J. Virol.* **78,** 11563–11573
18. Hachiya, A., Aizawa-Matsuoka, S., Tanaka, M., Takahashi, Y., Ida, S., Gatanaga, H., Hirabayashi, Y., Kojima, A., Tatsumi, M., and Oka, S. (2001) *Antimicrob. Agents Chemother.* **45,** 495–501
19. Stremlau, M., Perron, M., Lee, M., Li, Y., Song, B., Javanbakht, H., Diaz-Griffero, F., Anderson, D. J., Sundquist, W. I., and Sodroski, J. (2006) *Proc. Natl. Acad. Sci. U.S.A.* **103,** 5514–5519
20. Yee, J. K., Miyanohara, A., LaPorte, P., Bouic, K., Burns, J. C., and Friedmann, T. (1994) *Proc. Natl. Acad. Sci. U.S.A.* **91,** 9564–9568
21. Shen, M., Stukenberg, P. T., Kirschner, M. W., and Lu, K. P. (1998) *Genes Dev.* **12,** 706–720
22. Laurent, A. G., Krust, B., Rey, M. A., Montagnier, L., and Hovanessian, A. G. (1989) *J. Virol.* **63,** 4074–4078
23. Fuchigami, T., Misumi, S., Takamune, N., Takahashi, I., Takama, M., and Shoji, S. (2002) *Biochem. Biophys. Res. Commun.* **293,** 1107–1113
24. Wulf, G., Finn, G., Suizu, F., and Lu, K. P. (2005) *Nat. Cell Biol.* **7,** 435–441
25. Lu, K. P., Hanes, S. D., and Hunter, T. (1996) *Nature* **380,** 544–547
26. Ryo, A., Nakamura, M., Wulf, G., Liou, Y. C., and Lu, K. P. (2001) *Nat. Cell Biol.* **3,** 793–801
27. Zacchi, P., Gostissa, M., Uchida, T., Salvagno, C., Avolio, F., Volinia, S., Ronai, Z., Blandino, G., Schneider, C., and Del Sal, G. (2002) *Nature* **419,** 853–857
28. Liou, Y. C., Sun, A., Ryo, A., Zhou, X. Z., Yu, Z. X., Huang, H. K., Uchida, T., Bronson, R., Bing, G., Li, X., Hunter, T., and Lu, K. P. (2003) *Nature* **424,** 556–561
29. Gamble, T. R., Vajdos, F. F., Yoo, S., Worthylake, D. K., Houseweart, M., Sundquist, W. I., and Hill, C. P. (1996) *Cell* **87,** 1285–1294
30. Gamble, T. R., Yoo, S., Vajdos, F. F., von Schwedler, U. K., Worthylake, D. K., Wang, H., McCutcheon, J. P., Sundquist, W. I., and Hill, C. P. (1997) *Science* **278,** 849–853
31. Gitti, R. K., Lee, B. M., Walker, J., Summers, M. F., Yoo, S., and Sundquist, W. I. (1996) *Science* **273,** 231–235

Targeted Delivery of Immunogen to Primate M Cells with Tetragalloyl Lysine Dendrimer[1]

Shogo Misumi,[2]* Mitsuaki Masuyama,[2]*† Nobutoki Takamune,* Daisuke Nakayama,* Ryotarou Mitsumata,* Hirokazu Matsumoto,* Norimitsu Urata,* Yoshihiro Takahashi,† Atsunobu Muneoka,† Takayuki Sukamoto,† Koichiro Fukuzaki,† and Shozo Shoji[3]*‡

Effective uptake of Ags by specialized M cells of gut-associated lymphoid tissues is an important step in inducing efficient immune responses after oral vaccination. Although stable nontoxic small molecule mimetics of lectins, such as synthetic multivalent polygalloyl derivatives, may have potential in murine M cell targeting, it remains unclear whether synthetic multivalent polygalloyl derivatives effectively target nonhuman and human M cells. In this study, we evaluated the ability of a tetragalloyl derivative, the tetragalloyl-D-lysine dendrimer (TGDK), to target M cells in both in vivo nonhuman primate and in vitro human M-like cell culture models. TGDK was efficiently transported from the lumen of the intestinal tract into rhesus Peyer's patches by M cells and then accumulated in germinal centers. Oral administration of rhesus CCR5-derived cyclopeptide conjugated with TGDK in rhesus macaque resulted in a statistically significant increase in stool IgA response against rhesus CCR5-derived cyclopeptide and induced a neutralizing activity against SIV infection. Furthermore, TGDK was specifically bound to human M-like cells and efficiently transcytosed from the apical side to the basolateral side in the M-like cell model. Thus, the TGDK-mediated vaccine delivery system represents a potential approach for enabling M cell-targeted mucosal vaccines in primates. ***The Journal of Immunology,*** **2009, 182: 6061–6070.**

Human immunodeficiency virus is transmitted primarily via the genital mucosa during sexual intercourse. Elucidating the early events in mucosally transmitted HIV-1 infection plays a critical role in characterizing the virus-host interactions and effective vaccine design and development. Mucosal transmission of HIV-1 infection is mediated by exposure to cell-free viruses and/or cell-associated viruses within mucosal secretions, and established within hours, and can be disseminated to draining lymph nodes within days (1, 2). Recent studies of pathological events in acute infection in nonhuman primates and humans have provided important insights into the disruption of the mucosal immune system. This disruption is evident in the rapid depletion of $CD4^+$ T cells within the GALT during acute infection (3, 4), suggesting that once mucosal infection has occurred, immune responses to infection are insufficient to prevent these events. Therefore, a preventive vaccine should effectively target the earliest events in the establishment of HIV infection at the mucosal site.

Conventional vaccines administered from any routes other than the oral route effectively induce protective systemic immune responses, but the level of protective immunity at the major site of HIV mucosal entry is less robust. However, neutralizing Abs administered i.v. at high doses can reach mucosal sites and block genital mucosal transmission of simian/HIV (SHIV)[4] in nonhuman primate models (5), suggesting that sufficient mucosal humoral immune responses induced by mucosal vaccines can prevent HIV infection. Some related studies have shown that mucosal vaccines induce not only secretory IgA at mucosal sites, but also mucosal cell-mediated immunity and systemic Abs against HIV (6–13). These studies suggest that mucosal vaccines have several advantages over conventional systemic vaccines because they can induce multi-immuno responses that prevent HIV infection at the mucosal site.

Current efforts to develop effective mucosal vaccines are mainly directed toward finding more efficient means of delivering appropriate Ags to the mucosal immune system and toward developing effective and safe mucosal adjuvants (14) because it has often proved difficult to stimulate strong mucosal IgA immune responses and protection against pathogens by mucosal administration of Ags without Ag delivery and adjuvant systems. It is generally accepted that M cells in Peyer's patches (PPs) are instrumental in initiating mucosal immunity against pathogens invading across epithelial barriers (15). The high transcytotic abilities of M cells

*Department of Pharmaceutical Biochemistry, Faculty of Medical and Pharmaceutical Sciences, Kumamoto University, Kumamoto, Japan; †Shin Nippon Biomedical Laboratories, Kagoshima, Japan; and ‡Kumamoto Health Science University, Kumamoto, Japan

Received for publication September 3, 2008. Accepted for publication March 13, 2009.

The costs of publication of this article were defrayed in part by the payment of page charges. This article must therefore be hereby marked *advertisement* in accordance with 18 U.S.C. Section 1734 solely to indicate this fact.

[1] This study was supported in part by a Grant-in-Aid for scientific research from the Ministry of Education, Culture, Sports, Science, and Technology of Japan, and a health science research grant from the Ministry of Health, Labor, and Welfare of Japan.

[2] S.M. and M.M. contributed equally to this work.

[3] Address correspondence and reprint requests to Dr. Shozo Shoji, Kumamoto University, Department of Pharmaceutical Biochemistry, Faculty of Medical and Pharmaceutical Sciences, 5-1 Oe-Honmachi, Kumamoto 862-0973, Japan. E-mail address: shoji@gpo.kumamoto-u.ac.jp

[4] Abbreviations used in this paper: SHIV, simian/HIV; DAPI, 4′,6-diamidino-2 phenylindole; DIC, differential interference contrast; DMF, dimethylformamide; EDS, energy-dispersive x-ray spectroscopy; FAE, follicle-associated epithelium; Fmoc, 9-fuorenylmethoxycarbonyl; GC, germinal center; PEG, polyethylene glycol; PP, Peyer's patch; PV, poliovirus; rcDDR5, rhesus CCR5-derived cyclopeptide; RT, room temperature; SMPD, synthetic multivalent polygalloyl derivative; TEM, transmission electron microscopy; TGDK, tetragalloyl-D-lysine dendrimer; TRITC, tetramethylrhodamine isothiocyanate; UEA-1, *Ulex europaeus agglutinin-1*; wpim, weeks postinitial immunization.

www.jimmunol.org/cgi/doi/10.4049/jimmunol.0802928

make them an attractive target for mucosally delivered vaccines because mucus secretion may flush away an applied mucosal vaccine at the mucosal site. Some studies showed that mucosal vaccine delivery can be improved using appropriate bioadhesin molecules such as lectins because M cell surface glycocalyx differs in carbohydrate composition from that of enterocytes in many species (16–22). *Ulex europaeus agglutinin-1* (UEA-1)-conjugated (23, 24) or σ1 protein-conjugated nasal vaccination (13, 25) induces not only strong Ag-specific mucosal IgA and plasma IgG responses, but also CTL immunity. However, lectins such as UEA-1 are of limited value in vaccine delivery because they are toxic and subject to intestinal degradation. Lambkin et al. (26) reported that a stable low m.w. four-copy gallic acid construct is a competitor of UEA-1 and appears to have high affinity for the fucose receptor on murine M cells. Although stable nontoxic small molecular mimetics of UEA-1 have the potential for M cell targeting in mice, it remains unclear whether these mimetics effectively target the nonhuman and human M cells.

In this study, we synthesized the tetragalloyl-D-lysine dendrimer (TGDK) and demonstrated its M cell targeting potential in both in vivo nonhuman primate and in vitro human M-like cell culture models.

Materials and Methods

TGDK and D-lysine dendrimer

The 9-fuorenylmethoxycarbonyl (Fmoc)-D-MAP_4-NH-(CH_2)-NH-Trt-resin (in this study referred to as Fmoc-D-lysine dendrimer resin; Watanabe Chemical Industries) was treated with 20% piperidine/dimethylformamide (DMF) for 20 min to remove the Fmoc group. To prepare TGDK, the resin (0.51 mmol) was then washed five times with DMF and reacted with 3,4,5-trimethoxybenzoic acid chloride (1 mmol) in triethylamine (7 mmol) at 40°C for 120 min. The resulting resin was washed with 1% triethylamine/DMF three times and DMF five times, and then treated with boron tribromide (the amount is 20× mole equivalent of that of DMF in the reaction mixture) at 40°C for 5 min before air drying. TGDK was extracted with Milli-Q water, purified, and lyophilized. The patent for the synthesis method of TGDK has been obtained (PCT/JP2006/321720). The D-lysine dendrimer was obtained by treating the D-lysine dendrimer resin with acetic acid/trifluoroethanol/dichloromethane (1:1:8). The molecular masses of TGDK and D-lysine dendrimer were determined by MALDI-TOF mass spectrometry (Burker Franzen Analytik).

Animals and tissue samples

Purpose-bred female rhesus macaques (*Macaca mulatta*) obtained from a supplier in China (4–6 years old) were used for this study. This study (permission no. 19-137) was approved and conducted in accordance with the guidelines of the Animal Care and Use Committee of Kumamoto University.

Inoculation of TGDK

Rhesus macaques were fasted overnight. They were then inoculated with 1 ml of FITC-labeled TGDK solution (100 nmol) or 0.5 ml of 10 nm gold-labeled TGDK at a site in the ileum (15 cm from the cecum) after celiotomy under anesthesia induced by a s.c. injection of urethane (ethyl carbamate, 800 mg/ml; 1.5 ml/kg body weight; Wako Pure Chemical) solution and an i.v. injection of α-chloralose (Wako Pure Chemical; 20 mg/ml; 5.5 ml/kg body weight) into the cephalic vein.

Inoculation of poliovirus (PV)

Rhesus macaques were fasted overnight. They were then inoculated with PV solution at a site in the ileum (15 cm from the cecum), as described previously (27).

Collection of PPs

The rhesus monkeys were euthanized by exsanguination under anesthesia, and the part of the ileum (15 cm from cecum) including the inoculation site was collected. After washing the collected part of the ileum, the blocks of PPs were embedded in the OCT compound (Sakura Finetechnical) for immunofluorescence staining or fixed in ice-cold 3% glutaraldehyde/0.1 M sucrose/PBS (pH 7.4) for transmission electron microscopy and energy-dispersive x-ray spectroscopy.

Histopathological study

Tissue samples were fixed in 10% neutral buffered formalin and were trimmed, embedded in paraffin, sectioned, stained with H&E, and examined by light microscopy.

Immunofluorescence staining

To examine the binding and tissue localizations of TGDK, 5 μm frozen sections derived from rhesus macaques inoculated with FITC-labeled TGDK solution were fixed in cold acetone and blocked with 1% nonfat skim milk in PBS^-. FITC-labeled TGDK was detected using a rabbit anti-FITC Ab (Zymed Laboratories) for signal amplification and a tetramethylrhodamine isothiocyanate (TRITC)-labeled anti-rabbit IgG Ab or an Alexa488-labeled anti-rabbit IgG Ab as a secondary Ab. To further examine how TGDK is incorporated into the lymphoid organ, the sections were stained with a PE-labeled anti-CD20 Ab (BD Biosciences) or an anti-CD54 Ab (R&D Systems) labeled with Alexa555 using a Zenon mouse IgG labeling kit (Invitrogen).

To investigate whether gp2 was expressed in rhesus PP M cells, the sections were pretreated with 0.1% Triton X-100, which is used to solubilize the mucus, and then stained with an anti-PV Ab (II-MAP-01; Japan Poliomyelitis Research Institute) labeled with Alexa488 using a Zenon mouse IgG labeling kit (Invitrogen Corporation) or a rabbit anti-gp2 Ab (IMGENEX) labeled with Alexa555 using a Zenon rabbit IgG labeling kit (Invitrogen). To further examine how FITC-labeled TGDK specifically binds to PP M cells, the sections were also pretreated with 0.1% Triton X-100 and then stained with a rabbit anti-FITC Ab and Alexa488-labeled anti-rabbit IgG Ab as a secondary Ab or a rabbit anti-gp2 Ab (IMGENEX) labeled with Alexa555 using a Zenon rabbit IgG labeling kit (Invitrogen). Some sections were counterstained with 4′,6-diamidino-2 phenylindole (DAPI) to show nuclei.

After the staining, slides were washed and analyzed with a Keyence Biozero BZ-8000 (Keyence) and a Flowview FV3000 (Olympus).

Transmission electron microscopy (TEM) and energy-dispersive x-ray spectroscopy (EDS)

Tissue samples were rinsed in PBS with 0.1 M sucrose (pH 7.4) and post-fixed with 1% osmium tetroxide in 0.1 M phosphate buffer at 4°C for 2 h. All the samples were rinsed briefly with 50:50, 70:30, 80:20, 90:10, and 95:5 ethanol/water mixtures and 100% ethanol for 10 min each and three times with 100% ethanol for dehydration, and then embedded in epoxy resin (Quatol 812). One-micrometer sections were cut using a glass knife and then stained with toluidine blue. Suitable areas for ultrastructural study were chosen after examining 1-μm sections under a light microscope. Sections of 60–90 nm were cut on a Leica EM UC6 ultramicrotome using a diamond knife, and sections were mounted on a copper grid and stained with 1% uranyl acetate and Reynolds lead citrate. The grids were examined under a JEOL JEM 1200-EX electron microscope. Furthermore, EDS, which was consigned to JEOL Datum, was performed to quantify TGDK by measuring gold concentration within a specimen.

Preparation of TGDK-conjugated multiantigens

To examine the in vivo effect of TGDK on M cell targeting, TGDK was conjugated via a Hubantigen with rhesus CCR5-derived cyclopeptide (rcDDR5) and BSA. To prepare a Hubantigen, an eight-arm functional polyethylene glycol (PEG) with *p*-nitrophenyl groups, SUNBRIGHT HGEO-200NP (NOF Corporation; 1 equivalent), was mixed with an eight-arm functional PEG with primary amino groups, SUNBRIGHT HGEO-200PA (NOF; 7.2 equivalent), in DMF for 16 h. The resulting Hubantigen was dialyzed in Spectrapore dialysis bags (Spectrum Laboratories; molecular weight cut off = 12–14 kDa) against Milli-Q water for 2 days. The dialysate was lyophilized and used as a Hubantigen. To prepare rcDDR5, a rhesus CCR5-derived linear dodecapeptide (H_2N-KRSQREGLHYTG-COOH), in which all side-chain groups are protected, was synthesized using an automatic peptide synthesizer, and cyclized, as previously described (28). To bind both TGDK and rcDDR5 to the Hubantigen, the amino group of ethylenediamine in TGDK (two equivalents) or of Lys^1 in the deprotected rcDDR5 (two equivalents) was conjugated to four-armed functional PEG, SUNBRIGHT PTE-100NP (NOF; 1 equivalent). Finally, the Hubantigen (168 mg) was coupled to the four-armed PEG-ylated TGDK (12 μmol) and -rcDDR5 (12 μmol) in DMF for 24 h and then covalently bound to BSA for 6 h. The TGDK-conjugated Ag was dialyzed for 15 h against PBS^-, and the dialysate was lyophilized with lactose. The resulting Ag was encapsulated in enteric-coated capsules and included TGDK (56 nmol/capsule), rcDDR5 (90 nmol/capsule), lactose (146 μmol/capsule), and BSA (4.5 nmol/capsule). In contrast, a control Ag also included BSA (4.5 nmol/capsule), but it was not conjugated via a covalent

bond with a Hubantigen. Furthermore, the control Ag did not include TGDK and rcDDR5.

Immunization schedule

All of the rhesus macaques were housed in individual cages and maintained in accordance with the rules and guidelines of the National Institute for Infectious Diseases for experimental animal welfare. Five 4- to 6-year-old rhesus macaques (no. 6–10) were orally administered with two enteric-coated capsules containing TGDK-conjugated multiantigens at 0, 2, and 6 wk. Another five rhesus macaques (no. 1–5) were immunized with an enteric-coated capsule including control Ag following the same immunization schedule as that for the controls. Stool samples were obtained at 0, 12, 13, and 14 wk postinitial immunization (wpim), which were then subjected to anti-BSA Ab ELISA and rcDDR5-coupled multipin ELISA in accordance with the method of Misumi et al. (29).

Sample collection and processing

Acetone powder was prepared by adding fecal pellets (3 g) with stirring to 3 ml of cold acetone. The powder was then washed three times with cold ether and dried until no trace of ether remained. The acetone powder (100 mg) was resuspended in 400 μl of 1% MPC polymer solution (NOF) and incubated at 37°C for 30 min, and then on ice for 1 h. The suspensions were centrifuged at 13,000 × *g* for 5 min to remove fecal solids. The processed fecal Ab samples were subjected to anti-BSA Ab ELISA and rcDDR5-coupled multipin ELISA.

Anti-BSA Ab ELISA

Abs against BSA in stool samples were detected by ELISA. For evaluation of stool Abs, each well of a flat-bottom 96-well maxisorp microplate (Nunc) was coated with 50 μl of coating buffer (pH 8.0) containing BSA (100 μg/ml) and incubated at room temperature (RT) overnight. The wells were washed with 150 μl of Milli-Q water with 0.1% Tween 80 with complete decanting and rinsed with Milli-Q water. Subsequently, 100 μl of blocking buffer, composed of 1% skim milk in Milli-Q water, was added to each well and incubated for 2 h at RT to occupy all unbound sites. Washing was repeated, as described above, followed by the addition of 50 μl of a fecal Ab sample diluted 1/10 in PBS^- to each well. Plates were incubated for 2 h at RT and then washed with 0.1% Tween 80, and 50 μl of peroxidase-conjugated goat anti-monkey IgA (diluted 1/5000) was added to each well and incubated for 1 h at RT before the plate was washed. Fifty microliters 3,3′,5,5′-tetramethylbenzidine solution (Wako Pure Chemical) as the substrate was added to each well and incubated at room temperature. Absorbance was measured at 450/630 nm using a microplate reader.

rcDDR5-coupled multipin ELISA

A rhesus CCR5-derived linear dodecapeptide (H_2N-ERSQREGLHYTG-COOH) in which all side-chain groups are protected was synthesized using an automatic peptide synthesizer and was cyclized by bond formation between the α-carboxyl group of Gly and the α-amino group of Glu after removal of the resin. The γ-carboxyl group of Glu in the protected cyclic dodecapeptide was conjugated to MultiPin block (Mimotopes). The block was used for detecting anti-CCR5 Abs in stool samples in accordance with the method of Misumi et al. (28).

Determination of total number of SIV DNA copies

The total number of SIVmac239 DNA copies was determined to monitor SIV infection and estimate the neutralizing activity of antisera. The relative change in the number of SIV DNA copies indicates the degree of neutralizing activity. Percentage of copies in HSC-F infected with SIVmac239 in the presence of a 14-wpim stool sample is expressed relative to that in the presence of a 0-wpim stool sample, which is considered 100%. HSC-F cells (4×10^6) were infected with SIVmac239 (50 ng, measured using p27 Ag) in the presence of the 0- and 14-wpim stool samples, dialyzed (cutoff, 100 kDa) against PBS^-, and diluted in PBS^-. The inhibitory effect of the stool sample was investigated at 55-fold final dilution. After 48 h, HSC-F cells were harvested. The total viral DNA obtained after the purification procedure (29) was used for SYBR Green real-time PCR assay, as previously described (30), with some modifications. Briefly, primers that recognize specific and highly conserved sequences on the *gag* region of SIV described by Ui et al. (31) were selected. The sequences of SIV *gag* primers were 5′-GGAAATTACCCAGTACAACAAATAGG-3′ and 5′-TC TATCAATTTTACCCAGGCATTTA-3′. The SIV *gag* gene was amplified in 20 μl of a PCR mixture consisting of 10 μl of 2× master mix containing modified DyNAmo hot start DNA polymerase, SYBR Green I, optimized PCR buffer, 5 mM $MgCl_2$, a dNTP mix including dUTP (Finnzymes), 2 μl of each primer, and 8 μl of cDNA. PCR was conducted as follows: initial activation of hot start DNA polymerase at 95°C for 15 min; 40 cycles of four steps of 95°C for 10 s, 57°C for 20 s, 72°C for 20 s, and 76°C for 2 s. At the end of the amplification cycle, melting temperature analysis was conducted by gradually increasing temperature (0.5°C/s) to 95°C. Amplification, data acquisition, and analysis were conducted with the DNA Engine Opticon 2 System (Bio-Rad) using Opticon Monitor version 3.0 software.

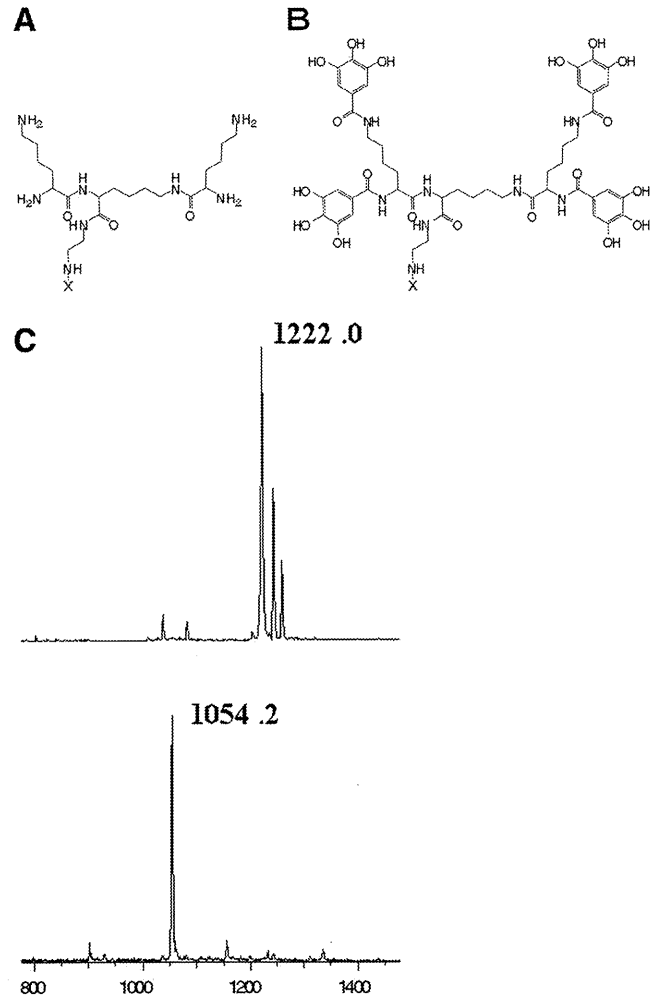

FIGURE 1. Structure and mass spectrometry of TGDK. *A*, D-lysine dendrimer. *B*, TGDK. *C*, MALDI-TOF mass spectrometry spectrum of intermediate compound, $(3,4,5\text{-trimethoxybenzoyl})_4$-D-lyseine dendrimer, and TGDK. The spectra exhibited two peaks at m/z 1222.0 and 1054.2: the *upper peak* is that of the ion derived from the reaction intermediate, $(3,4,5\text{-trimethoxybenzoyl})_4$-D-lyseine dendrimer, and the *lower peak* is that of the ion derived from TGDK.

In vitro human M cell model

The human M cell model was constructed using cocultures of Caco-2 cells and Raji cells in accordance with the method of Kernéis et al. (32) with slight modification. We seeded Caco-2 cells by adding 1×10^6 cells on the lower face of 3-μm-pore Transwell filters and culturing them overnight. The filters were then transferred to the Transwell device with the epithelial cells facing the lower chamber of the cluster plates. Caco-2 cells were cultured until they were fully differentiated (21 days). Raji B cells (10^6) were added to the upper chamber facing the basolateral side of Caco-2 cells. The cultures were maintained for 3 days. Caco-2 cell monolayers were washed with PBS^- and incubated with FITC-labeled TGDK, or FITC-labeled D-lysine dendrimer with or without PV (type II, $10^{4.5}$–$10^{5.5}$ cell culture infective doses 50%) for 30 min. To examine the localization of PV and M cell makers (i.e., gp2, CD54, and integrin β_1), the monolayers were stained with an anti-PV Ab (II-MAP-01; Japan Poliomyelitis Research Institute), an anti-gp2 polyclonal Ab (IMGENEX) labeled with

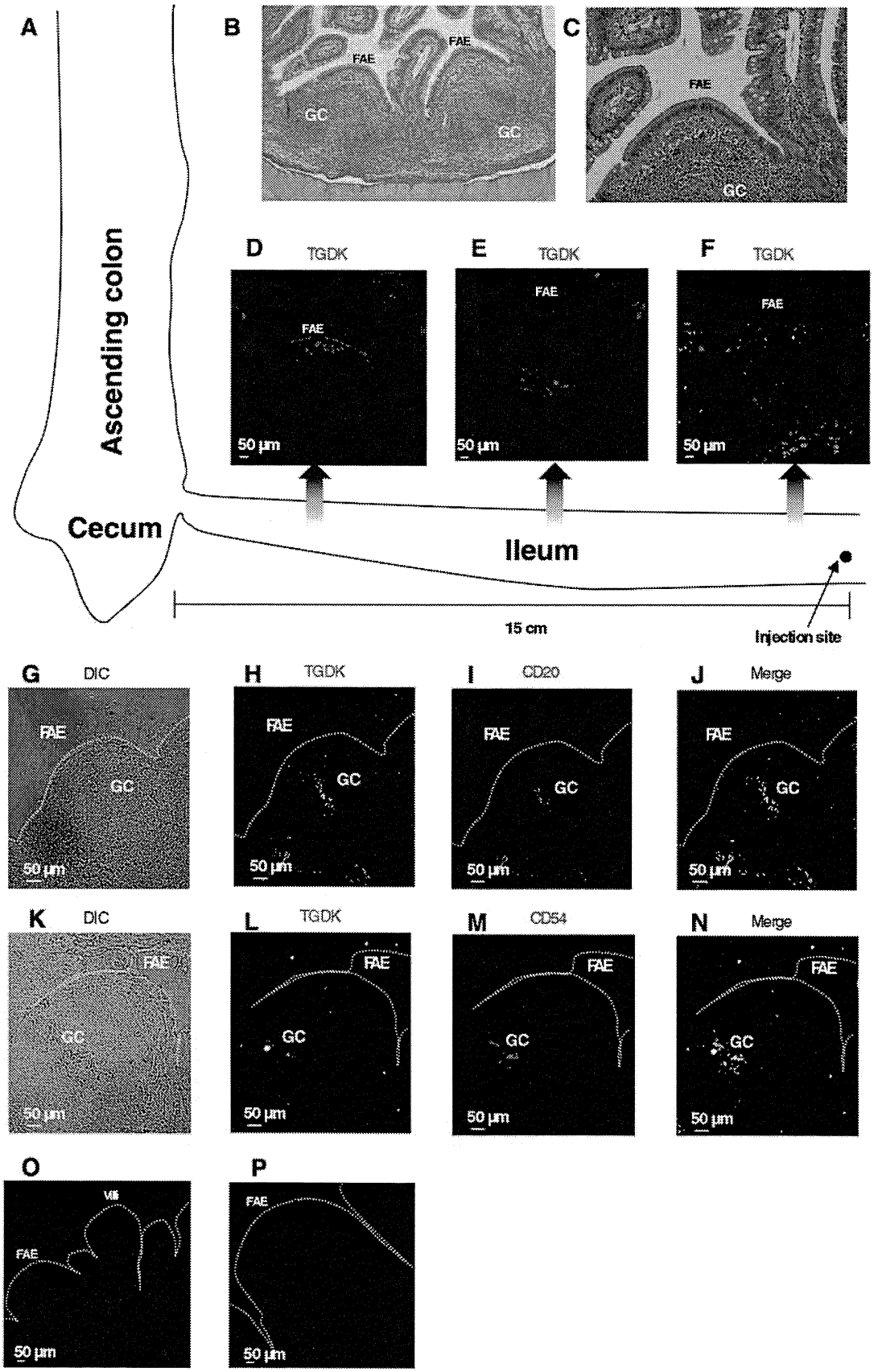

FIGURE 2. Association of TGDK with rhesus PP FAE and accumulation of TGDK within the GCs. *A*, Schematic diagram of rhesus ileum. *B* and *C*, H&E staining of rhesus PPs. *D–F*, FITC-labeled TGDK was inoculated into the lumen of the ileum at 15 cm from the ileocecal valve. One hour after TGDK inoculation, the portion between the injection site of TGDK and the ileocecal valve was excised and subjected to immunofluorescence analysis. Frozen sections of rhesus macaque PPs were labeled with mAbs (anti-CD20 Ab (*I*) and anti-CD54 Ab (*M*); red), and TGDK was stained, as described in *Materials and Methods* (red or green) (*D–F*, *H*, and *L*). Differential interference contrast (DIC) (*G* and *K*), merged (*J* and *N*), and control (*O*, Alexa488-labeled anti-rabbit IgG, or *P*, TRITC-labeled anti-rabbit IgG) images are shown.

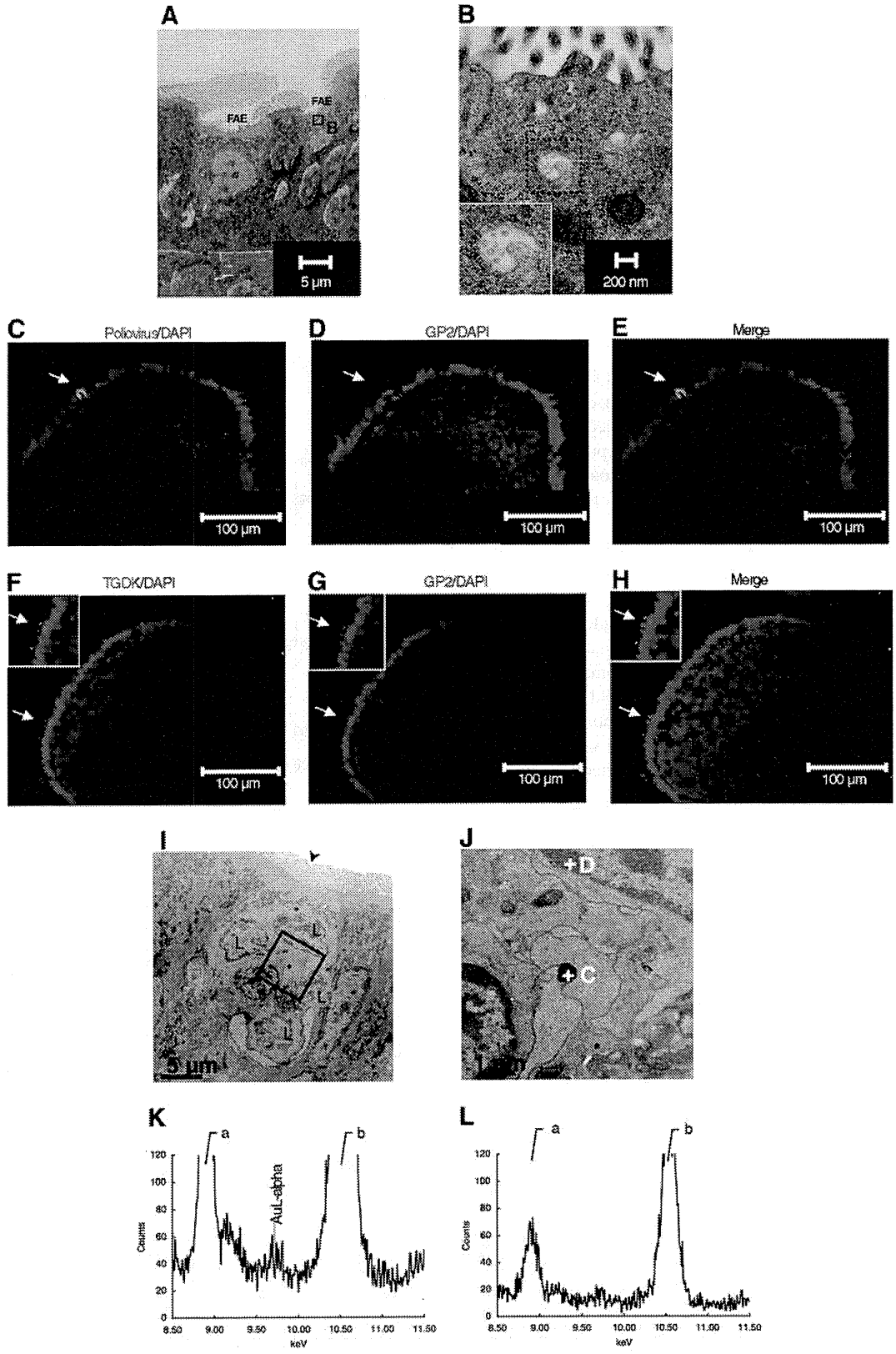

FIGURE 3. TGDK can efficiently penetrate into rhesus PP M cells. PV, FITC-labeled TGDK, or 10-nm gold-labeled TGDK was inoculated into the lumen of the ileum, as described in *Materials and Methods*. After the inoculation, the portion between the inoculation site and the ileocecal valve was excised and subjected to electron microscopies (*A*, *B*, *I*, and *J*), immunofluorescence analysis (*C–H*), or EDS (*K* and *L*). *A*, TEM image of typical M cells in the PP. *B*, TEM image of *B* shown in *A*. *Inset* (the magnified TEM image of dotted square in *B*), PV is transcytosed through rhesus PP M cells. *C–H*, Frozen sections of rhesus macaque PPs were labeled with mAbs (anti-PV Ab (*C*) and anti-gp2 Ab (*D* and *G*)), and TGDK were stained, as described in *Materials and Methods* (*F*). Merged images are shown (*E* and *H*). *I*, TEM view of rhesus PP M cells, which had short (arrowhead) and irregular microvilli and pocket structures containing lymphocytes (indicated by *L*). *J*, Depicts a higher-magnification image of *I*. *K* and *L*, Graphs show EDS of *spots C* and *D* in *J*, confirming the presence of gold-labeled TGDK. The *a* signals come from Cu (8.904 keV), which is attributed to the sample holder, and the *b* signal contains the signal of OsLβ (10.354 keV).

Alexa555 using a Zenon mouse IgG labeling kit (Invitrogen), a mouse anti-human CD54 Ab (R&D Systems), or a mouse anti-human integrin $\alpha_5\beta_1$ Ab (Chemicon International), and then incubated with or without TRITC-labeled goat anti-mouse IgG (Jackson ImmunoResearch Laboratories). At the end of the staining, slides were washed and incubated with DAPI for nuclear staining. Finally, the monolayers were washed and analyzed with a Keyence Biozero BZ-8000. To investigate whether TGDK was specifically transported in human M cell model, the assay was conducted in the presence of 100 μM FITC-labeled TGDK or FITC placed in the lower chamber. The monolayers including M cells or Caco-2 control monolayers were incubated for 2 h at 37°C. FITC-labeled TGDK or FITC, transported from the lower chamber to the upper chamber, was quantified using a CORONA Multi Microplate Reader.

Results

Synthesis of TGDK

UEA-1, an α-L-fucose-specific lectin, has been of particular interest owing to its M cell specificity in the mouse model and its applicability to proof-of-concept studies of vaccine delivery to APCs (33). However, lectins are susceptible to proteolytic degradation in the gastrointestinal tract, and their cytotoxic effects also limit their use as targeting agents to deliver vaccines to M cells. One approach to overcoming these limitations is to synthesize small organic molecules that are able to mimic the function of lectins. Lambkin et al. (26, 34) reported that a synthetic multivalent polygalloyl derivative (SMPD) is a competitor of UEA-1 and appears to have high affinity for the fucose receptor on murine M cells. Its advantages include its stability and suitability for incorporation into delivery systems using routine chemical procedures. In this study, we also chose a versatile scaffold with branched D-lysine (Fig. 1*A*). An aminoethyl group was introduced into the lysine dendrimeric scaffold to allow its linkage with a candidate immunogen. Furthermore, gallic acid was selected as a polyphenolic functional group and coupled with α- and ε-amino groups of lysine residues in the lysine dendrimer (Fig. 1*B*). As shown in Fig. 1*C*, the spectra of purified $(3,4,5\text{-trimethoxybenzoyl})_4$-D-lysine dendrimer and TGDK exhibited major peaks at m/z 1222.0 (Fig. 1*C*, *upper spectrum*) and 1054.2 (Fig. 1*C*, *lower spectrum*), respectively. The difference in molecular mass indicates the complete deprotection of the methyl group by boron tribromide.

TGDK transport through follicle-associated epithelium (FAE) of rhesus macaque PPs

To examine whether TGDK was effectively transported through FAE of PPs in vivo, FITC-labeled TGDK was inoculated into the rhesus macaque ileum (Fig. 2*A*). One hour after the injection, the tissue was subjected to immunofluorescence analysis. As shown in Fig. 2, *B* and *C*, the large PP is found in the lumen of the terminal ileum in rhesus macaques. Light microscopy revealed the typical structure of a mucosal lymphoid follicle, composed of germinal centers (GCs) and a dome area bulging into the lumen (Fig. 2, *B* and *C*). The closer the section to the injection site, the larger the amount of TGDK reaching GCs through FAE of PPs (Fig. 2, *D–F*). When PPs from different sections (~7.5 cm from the injection site) were further observed, TGDK was clearly detected in the GCs of PPs (Fig. 2, *H* and *L*). GC cells can be stained with anti-CD20 and anti-CD54 Abs, the staining patterns reflecting reactivity with B cell lymphocytes and the follicular dendritic reticulum in nonhuman primates and humans, respectively (35–37). As shown in Fig. 2, *I* and *M*, CD20 and CD54 were expressed within the GCs of rhesus macaques. Fig. 2, *J* and *N*, shows the patterns of double fluorostaining for TGDK/CD20 or TGDK/CD54 in the GCs of PPs. These results indicate that TGDK efficiently enters into GCs through FAE of PPs in rhesus macaques.

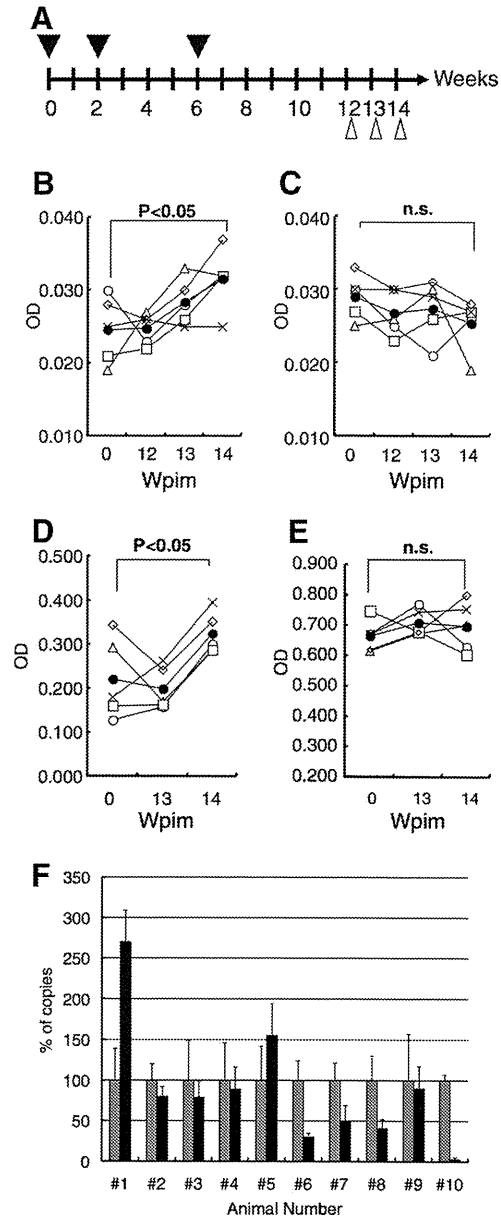

FIGURE 4. Oral immunization schedule and detection of anti-BSA or anti-rcDDR5 Abs in rhesus macaques. *A*, Immunization schedule for rhesus macaques. Five rhesus macaques (no. 6–10) were orally immunized at 0, 2, and 6 wk with TGDK-conjugated multiantigens. Another five macaques (no. 1–5) were immunized with the control Ag. Stool sampling was performed at 12, 13, and 14 wpim. Stool samples (1/10 dilution) obtained after immunization with TGDK-conjugated multiantigen (*B*; macaque no. 6 (○), 7 (△), 8 (■), 9 (◇), and 10 (×)) or control Ag (*C*; macaque no. 1 (○), 2 (△), 3 (■), 4 (◇), and 5(×)) were examined to investigate whether the anti-BSA mucosal IgA (*B* and *C*) or anti-rcDDR5 mucosal IgA (*D* and *E*) can be raised in rhesus macaques by anti-BSA ELISA and the rcDDR5-coupled multipin ELISA, as described in *Materials and Methods*. ○, Show the average OD values. *F*, Furthermore, the inhibitory effect of the stool samples from vaccinated (no. 6–10) and control groups (no. 1–5) on in vitro SIV infection was also investigated, as described in *Materials and Methods*. Percentage of copies in HSC-F infected with SIVmac239 in the presence of the 14-wpim stool sample (■) is expressed relative to that in the presence of the 0-wpim stool sample (▨), which is considered 100%.

Internalization of TGDK by PP M cells

To investigate whether rhesus macaque PP M cells can specifically take up TGDK, the rhesus macaque ileum was inoculated with FITC-labeled TGDK and subjected to immunofluorescence

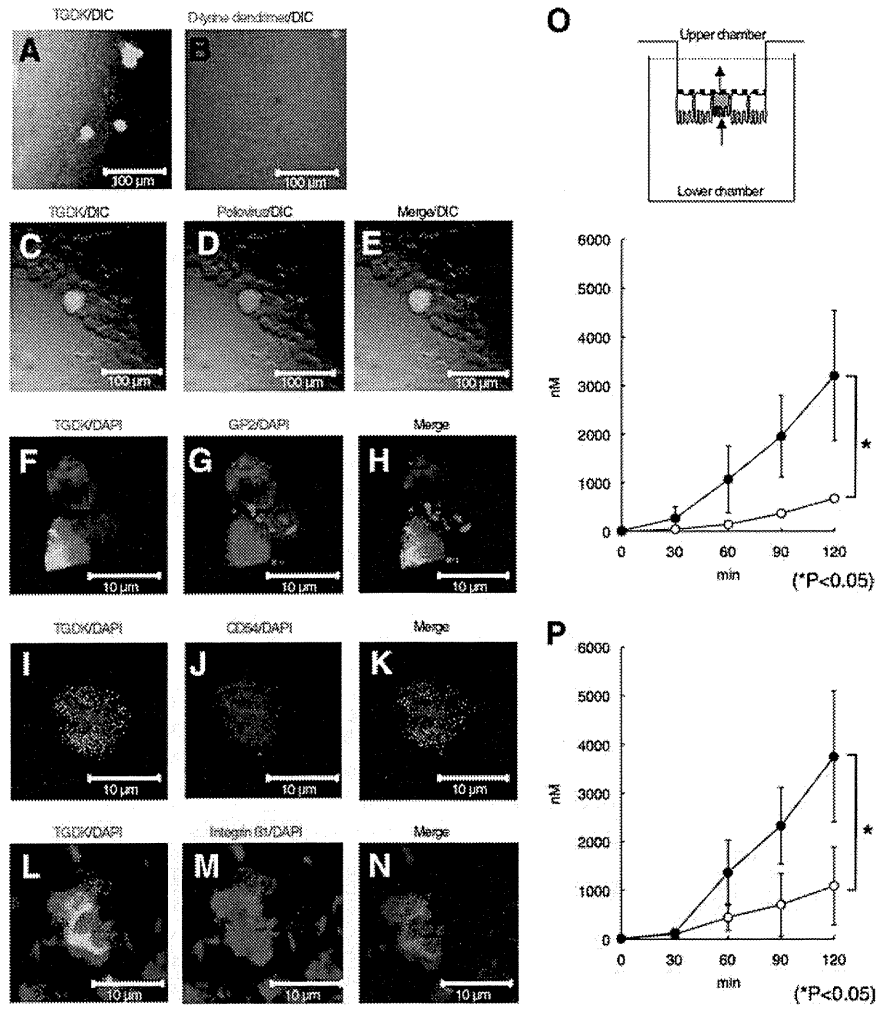

FIGURE 5. Association of TGDK with human M-like cells and transcytosis of TGDK. The Caco-2/Raji B monolayer was stained with FITC-labeled TGDK (*A*, *C*, *F*, *I*, and *L*, green) or the FITC-labeled D-lysine dendrimer (*B*, green), as described in *Materials and Methods*. Because it is known that PV can bind to M-like cells, the Caco-2/Raji B monolayer was labeled with an anti-PV Ab (*D*, red). The monolayer was further labeled with mAbs (anti-gp2 (*G*), anti-CD54 (*J*), and anti-integrin β_1 Abs (*M*), red). *A* and *C*, Show the merge image of DIC and a fluorescence image of FITC-labeled TGDK. *B*, Shows the merge image of DIC and a fluorescence image of FITC-labeled D-lysine dendrimer. *D*, Shows the merge image of DIC and a fluorescence image of monolayer labeled with an anti-PV Ab. *F*, *I*, and *L*, Show the patterns of double fluorostaining for TGDK/DAPI. *G*, *J*, and *M*, Show the patterns of double fluorostaining for gp2/DAPI, CD54/DAPI, and integrin β_1/DAPI. Furthermore, merged (*E*, *H*, *K*, and *N*) images are shown. *O*, To investigate the transcytosis activity of TGDK, the monolayers including M-like cells (●) or Caco-2 control monolayers (○) were incubated with FITC-labeled TGDK. *P*, To investigate the transcytosis efficacy of TGDK, the monolayers including M-like cells were incubated with FITC-labeled TGDK (●) or FITC (○). FITC-labeled TGDK or FITC transported from the lower chamber to the upper chamber was quantified by a CORONA Multi Microplate Reader.

analysis (Fig. 3). Recently, Terahara et al. (38) reported that gp2 is specifically expressed at a high level in mouse PP M cells. However, the expression of gp2 in rhesus PP M cells remains to be clarified in rhesus macaque. Sicinski et al. (39) reported that PV is found specifically adhering to the surface projections of M cells and in vesicles in M cells. Fig. 3*A* shows a typical TEM image of PP M cells. As expected, PV was transcytosed through typical intestinal rhesus PP M cells (Fig. 3*B*). Therefore, we confirmed whether gp2 was expressed in rhesus PP M cells, in which PV was transcytosed. Immunofluorescence analysis demonstrated that gp2 was expressed in rhesus PP M cells (Fig. 3*D*), which were recognized by the anti-PV Ab (Fig. 3*C*). These results indicated that gp2 was expressed in rhesus PP M cells. To further investigate whether TGDK specifically binds to PP M cells, the localization of TGDK was confirmed by counterstaining with the anti-gp2 Ab. As shown in Fig. 3, *F* and *G*, TGDK was colocalized with gp2. These results indicated that TGDK specifically binds to rhesus M cells.

To investigate whether TGDK is transcytosed through PP M cells, the rhesus macaque ileum was inoculated with gold-labeled TGDK and subjected to EDS (Fig. 3). The advantage of EDS is that gold-labeled TGDK can be directly detected when TGDK is completely embedded in an ultrathin section. The characteristic x-ray peak from gold (AuL-α: ~9.712 keV) is used to confirm the presence of nano-gold particles in the cytoplasm of a PP M cell within a section (Fig. 3*I*). EDS demonstrated the presence of gold-labeled TGDK in the cytoplasm of a PP M cell (*spot C*; Fig. 3, *J* and *K*), but not in the cytoplasm of a lymphocyte within a PP M cell (*spot D*; Fig. 3, *J* and *L*). In contrast, gold-labeled TGDK was not detected in intestinal epithelial cells in FAE of PPs. Taken together, these results indicate that inoculation of TGDK into the rhesus macaque ileum containing PPs shows the clear targeting of M cells and transcytosis of TGDK, and rhesus macaque PP M cells have the ability to take up TGDK from the lumen.

Immunization of rhesus macaques with TGDK-conjugated multiantigens and induction of BSA- and rcDDR5-specific Abs

To examine the in vivo effect of TGDK on M cell targeting in nonhuman primates, five rhesus macaques were immunized with TGDK-conjugated multiantigens containing BSA and rcDDR5 by oral administration according to the time schedule shown in Fig. 4*A*. Another five rhesus macaques were immunized with the control Ag. Although BSA-specific IgA in stool samples was significantly induced in the group immunized with TGDK-conjugated multiantigens at 14 wpim (Fig. 4*B*; $p < 0.05$ in repeated measures ANOVA), the immunization with the TGDK-conjugated multiantigen unfortunately induced only weak anti-BSA Ab responses. The result suggests that the induction of a stronger anti-BSA Ab response may be required for a higher content of BSA in the TGDK-conjugated multiantigen. In contrast, the immunization of rhesus macaques with the control Ag did not induce BSA-specific IgA in stool samples (Fig. 4*C*).

Our previous studies demonstrated that the rhesus macaque antisera raised against cDDR5 mimicking the conformation-specific domain of human CCR5 reacted with both human and macaque CCR5s, and potently suppressed infection by the R5 HIV-1 laboratory isolate (HIV_{JRFL}), R5 HIV-1 primary isolates (clade

A:$HIV_{93RW004}$ and clade C:HIV_{MJ4}), and a pathogenic $SHIV_{SF162P3}$ bulk isolate in vitro (29). In addition, our recent data demonstrate that mouse anti-rcDDR5-specific IgG can inhibit in vitro SIV infection (40). Therefore, the stool samples from the group immunized with TGDK-conjugated multiantigens were also examined by rcDDR5-coupled multipin ELISA to determine whether rcDDR5-specific mucosal IgA was induced. As shown in Fig. 4*D*, rcDDR5-specific IgA in stool samples was significantly induced in the group immunized with TGDK-conjugated multiantigens. In contrast, the immunization of rhesus macaques with the control Ag did not induce rcDDR5-specific IgA in stool samples (Fig. 4*E*). Although we investigated whether rcDDR5-specific mucosal IgM or IgG was also induced, the rcDDR5-specific IgM or IgG in stool samples was not significantly induced (data not shown). To further assess neutralizing activity, we performed an in vitro neutralization assay using SIVmac239. Interestingly, neutralizing activity tended to increase with the titer of the anti-rcDDR5 IgA in stool samples (Fig. 4*F*). These data suggest that TGDK-mediated vaccine delivery system represents a potential approach to develop M cell-targeted mucosal vaccines.

Selective binding and transcytosis of TGDK in human in vitro M cell model

Although TGDK promises to be an M cell targeting molecule in nonhuman primates, it still remains unclear whether TGDK effectively targets human M cells. Kernéis et al. (32) developed an in vitro human M cell model that is useful for facilitating the design of oral vaccines and efficient mucosal drug delivery systems. Therefore, we evaluated whether TGDK selectively binds to human M-like cells and is capable of transcytosis. As shown in Fig. 5, *A* and *B*, the spotlike staining of the apical surface of epithelial cells in the model with the FITC-labeled TGDK was observed, but hardly in the model with the FITC-labeled D-lysine dendrimer. Because Sicinski et al. (39) demonstrated that PV enters the human host through intestinal M cells, we examined whether TGDK can colocalize with PV on the apical surface of the model (Fig. 5, *C—E*). Immunofluorescence analysis demonstrated that M cells in the model showed costaining of TGDK and PV. Furthermore, because human M cells express gp2, CD54, and $\alpha_5\beta_1$ integrin on their surface, the apical surface of epithelial cells in the model was also stained with the anti-gp2, anti-CD54, or anti-$\alpha_5\beta_1$ integrin Ab (Fig. 5, *G*, *J*, and *M*) (41–43). Fig. 5, *G*, *J*, and *M*, shows that gp2, CD54, and $\alpha_5\beta_1$ integrin are expressed on the apical surface. Fig. 5, *H*, *K*, and *N*, shows the patterns of triple fluorostaining for TGDK/gp2/DAPI, TGDK/CD54/DAPI, or TGDK/$\alpha_5\beta_1$ integrin/DAPI in this model.

Transcytotic activity was also monitored for 120 min at 37°C. TGDK was effectively transported at 37°C through the monolayers containing M cells, but not through control monolayers (Fig. 5*O*; $p < 0.05$ in Mann-Whitney *U* test). To further confirm TGDK-mediated Ag transport, we investigated whether FITC-labeled TGDK is more efficiently transported than FITC, which is postulated as an Ag. As shown in Fig. 5*P*, FITC-labeled TGDK is more efficiently transported than FITC ($p < 0.05$ in Mann-Whitney *U* test). These results indicate that TGDK can significantly bind to human M cells and is capable of transcytosis through M cells in inductive sites, such as PPs.

Discussion

The sexual route is the most important route of HIV transmission in heterosexuals, in which the genital tract provides the virus access to lymphoid cells. In the majority of patients, the initial acquisition of HIV involves passage of the virus across a mucosal surface. Thus, blocking HIV mucosal transmission is key to prevent HIV infection.

Some studies demonstrated that mucosal Ab responses may contribute to the apparent resistance to HIV-1 infection. The studies, in which humoral and cellular responses against HIV-1 in the vaginal secretions of women who remain uninfected despite frequent unprotected sex with HIV-1-infected partners were analyzed, indicated the presence of mucosal IgA Abs to HIV-1 (44–46). Furthermore, the second type of natural resistance is found in persons with CCR5-specific mucosal autoantibodies (47). To attempt to reproduce some of the functional aspects of this natural resistance to HIV infection, many researchers have examined various types of mucosal vaccine candidate against SIV/SHIV infection because they are capable of inducing not only the immunity at the mucosal sites of transmission, which prevents the virus from gaining entry into immune cells, but also the immunity in the systemic circulation.

Could CCR5 be an attractive target for the development of mucosal vaccines? Persons with the homozygous δ32 CCR5 mutation, a 32-bp deletion of the CCR5 gene that results in a lack of cell surface expression of CCR5, have strongly reduced susceptibility to CCR5-dependent HIV-1 infection (48–50). Furthermore, Pastori et al. (51) reported that long-lasting CCR5 internalization by anti-CCR5 Abs in a subset of long-term nonprogressors is associated with a possible protective effect against disease progression, suggesting that induction of anti-CCR5 Abs by a vaccine can reproduce the immune status in long-term nonprogressors. Our previous study demonstrated that the high induction of the anti-CCR5 Ab can suppress viral propagation during acute HIV-1 i.v. transmission in cynomolgus macaques i.p. and s.c. immunized with cDDR5 mimicking the conformation-specific domain of human CCR5 (29). In this study, rcDDR5 was synthesized to induce more specific anti-rhesus CCR5 Abs. Our recent study demonstrates that the immunization of rcDDR5-conjugated KLH induces mouse anti-rcDDR5-specific IgG that specifically binds to rhesus CCR5 and inhibits in vitro SIV infection (40). These observations suggest that CCR5 can be an attractive target for the development of mucosal vaccines. Hence, to reproduce the functional aspects found in long-term nonprogressors with CCR5-specific mucosal autoantibodies, we sought new types of vaccine delivery system for the effective delivery of rcDDR5 to mucosa-associated lymphoid tissues such as PPs, the inductive site for the induction of the Ag-specific immune response.

Lectins have been investigated for targeted Ag delivery to mucosa-associated lymphoid tissues. UEA-1 and *Aleuria aurantia* lectin have high specificity for the carbohydrate moiety α-L-fucose located on the apical membranes of mouse M cells (19, 21, 52). There have been successful efforts made in in vivo targeting in mouse M cells by conjugating UEA-1 to polymerized liposomes (33) and latex particles (53), or by coating poly(D, L-lactide-co-glycolide) particles with the *A. aurantia* lectin (52). However, lectins are of limited value in vaccine delivery owing to their toxicity to humans or sensitivity to intestinal degradation. To overcome these limitations, SMPDs that appear to have high affinity for the fucose receptor on murine M cells were identified from a high-throughput screening of mixture-based compound libraries in a competitive UEA-1-binding assay (26). Although SMPDs may have the potential in oral vaccine targeting in mouse model, it remained unclear whether SMPDs effectively target nonhuman and human M cells.

The macaque model serves several important purposes in current HIV vaccine research. It allows analysis of vaccine safety and proof of immunogenicity in a species more closely related to humans. Furthermore, there are a few interesting options for testing

the effect of a vaccine on a mucosal pathogenic challenge system, such as SIV or SHIV challenges. Therefore, we investigated the M cell targeting potential of a tetragalloyl derivative, TGDK, in an in vivo nonhuman primate model. Our findings suggest that TGDK can serve as a useful targeting molecule for nonhuman primate M cells (Fig. 3). Interestingly, TGDK accumulated in GCs after it transcytosed through M cells from the gut lumen (Fig. 2, *D–F*). Although the mechanism underlying the behavior of TGDK in PP still remains to be elucidated, the ability of TGDK to accumulate in GCs may increase the possibility of interaction of an immunogen, in the form of an immune complex trapped on follicular dendritic cells, with GC B cells.

To assess the efficiency of TGDK as a mucosal delivery system, it is important to examine whether rcDDR5-specific Abs in mucosal secretions are induced in nonhuman primate models. It is generally difficult to induce a long-lasting anti-CCR5 Ab response because CCR5 is continuously exposed to the immune system. Our previous study showed that immunization with cDDR5-MAP induces anti-CCR5 serum production for ~15 wk after the third immunization, although the titer of anti-CCR5 sera declined over time until 21 wpim (29), suggesting that cDDR5-MAP is not suitable as a model Ag for the estimation of TGDK owing to its weak immunogenicity. Therefore, we introduced BSA as a standard model Ag into TGDK-conjugated multiantigens with rcDDR5 via the Hubantigen to estimate the efficiency of TGDK. Furthermore, our recent data indicate that anti-rcDDR5 serum is produced for more than 56 wk when rhesus macaques were inguinally immunized with the TGDK-conjugated multiantigens containing rcDDR5 and BSA without a specific adjuvant (our unpublished data), suggesting that the immunogenicity of TGDK-conjugated multiantigens used to evaluate the effect of TGDK was improved. Five animals were orally immunized with the TGDK-conjugated multiantigen (vaccinated group), and another five were immunized with the Hubantigen and BSA only (control group). Although the immunization with the TGDK-conjugated multiantigen induced only weak anti-BSA Ab responses in the vaccinated group (Fig. 4*B*; $p < 0.05$), rcDDR5-specific IgA in stool samples was significantly induced in the vaccinated group, as shown in Fig. 4*D*. Furthermore, the neutralizing activity tended to increase with the titer of the anti-rcDDR5 Ab in the stool samples (Fig. 4*F*). Taken together, these results show that TGDK is useful for inducing rcDDR5-specific mucosal IgA responses with neutralizing activity, although it is necessary to re-examine the dose of the orally administered TGDK-conjugated multiantigens for the perfect reproduction of the functional aspects found in long-term nonprogressors with CCR5-specific mucosal autoantibodies.

Finally, we examined whether TGDK can be available for human use using the human in vitro M cell model. Giannasca et al. (54) reported that the UEA-1 receptor is not expressed in human PPs, whereas Sharma et al. (55) reported that the UEA-1 binding was observed in M cells of human FAE. Because it further remained unclear whether the binding receptor of UEA-1 is completely the same as that of TGDK, we examined whether TGDK was directly capable of binding to human M-like cells. As shown in Fig. 5, TGDK can specifically bind to human M-like cells and transcytose through M-like cells. These results suggest that the TGDK-mediated vaccine delivery system can be available for mucosal vaccine delivery in humans.

Acknowledgments

We thank Dr. H. Matsunaga (Kumamoto University) for excellent technical assistance in TGDK synthesis. We thank K. Matsuda (Keyence) for excellent technical assistance in immunofluorescence analysis. We thank K. Nozaki, Y. Kudo, H. Kai, and K. Matsuura for excellent technical assistance in in vitro experiments.

Disclosures

The authors have no financial conflict of interest.

References

1. Pope, M., and A. T. Haase. 2003. Transmission, acute HIV-1 infection and the quest for strategies to prevent infection. *Nat. Med.* 9: 847–852.
2. Lackner, A. A., and R. S. Veazey. 2007. Current concepts in AIDS pathogenesis: insights from the SIV/macaque model. *Annu. Rev. Med.* 58: 461–476.
3. Li, Q., L. Duan, J. D. Estes, Z. M. Ma, T. Rourke, Y. Wang, C. Reilly, J. Carlis, C. J. Miller, and A. T. Haase. 2005. Peak SIV replication in resting memory $CD4^+$ T cells depletes gut lamina propria $CD4^+$ T cells. *Nature* 434: 1148–1152.
4. Guadalupe, M., E. Reay, S. Sankaran, T. Prindiville, J. Flamm, A. McNeil, and S. Dandekar. 2003. Severe $CD4^+$ T-cell depletion in gut lymphoid tissue during primary human immunodeficiency virus type 1 infection and substantial delay in restoration following highly active antiretroviral therapy. *J. Virol.* 77: 11708–11717.
5. Mascola, J. R., G. Stiegler, T. C. VanCott, H. Katinger, C. B. Carpenter, C. E. Hanson, H. Beary, D. Hayes, S. S. Frankel, D. L. Birx, and M. G. Lewis. 2000. Protection of macaques against vaginal transmission of a pathogenic HIV-1/SIV chimeric virus by passive infusion of neutralizing antibodies. *Nat. Med.* 6: 207–210.
6. Belyakov, I. M., B. Moss, W. Strober, and J. A. Berzofsky. 1999. Mucosal vaccination overcomes the barrier to recombinant vaccinia immunization caused by preexisting poxvirus immunity. *Proc. Natl. Acad. Sci. USA* 96: 4512–4517.
7. Gherardi, M. M., E. Perez-Jimenez, J. L. Najera, and M. Esteban. 2004. Induction of HIV immunity in the genital tract after intranasal delivery of a MVA vector: enhanced immunogenicity after DNA prime-modified vaccinia virus Ankara boost immunization schedule. *J. Immunol.* 172: 6209–6220.
8. Douce, G., V. Giannelli, M. Pizza, D. Lewis, P. Everest, R. Rappuoli, and G. Dougan. 1999. Genetically detoxified mutants of heat-labile toxin from *Escherichia coli* are able to act as oral adjuvants. *Infect. Immun.* 67: 4400–4406.
9. Belyakov, I. M., S. A. Hammond, J. D. Ahlers, G. M. Glenn, and J. A. Berzofsky. 2004. Transcutaneous immunization induces mucosal CTLs and protective immunity by migration of primed skin dendritic cells. *J. Clin. Invest.* 113: 998–1007.
10. Kang, S. M., Q. Yao, L. Guo, and R. W. Compans. 2003. Mucosal immunization with virus-like particles of simian immunodeficiency virus conjugated with cholera toxin subunit B. *J. Virol.* 77: 9823–9830.
11. Guo, L., X. Lu, S. M. Kang, C. Chen, R. W. Compans, and Q. Yao. 2003. Enhancement of mucosal immune responses by chimeric influenza HA/SHIV virus-like particles. *Virology* 313: 502–513.
12. Sakaue, G., T. Hiroi, Y. Nakagawa, K. Someya, K. Iwatani, Y. Sawa, H. Takahashi, M. Honda, J. Kunisawa, and H. Kiyono. 2003. HIV mucosal vaccine: nasal immunization with gp160-encapsulated hemagglutinating virus of Japan-liposome induces antigen-specific CTLs and neutralizing antibody responses. *J. Immunol.* 170: 495–502.
13. Wang, X., D. M. Hone, A. Haddad, M. T. Shata, and D. W. Pascual. 2003. M cell DNA vaccination for CTL immunity to HIV. *J. Immunol.* 171: 4717–4725.
14. Holmgren, J., C. Czerkinsky, K. Eriksson, and A. Mharandi. 2003. Mucosal immunization and adjuvants: a brief overview of recent advances and challenges. *Vaccine* 21(Suppl. 2): S89–S95.
15. Kraehenbuhl, J. P., and M. R. Neutra. 2000. Epithelial M cells: differentiation and function. *Annu. Rev. Cell. Dev. Biol.* 16: 301–332.
16. Jepson, M. A., M. A. Clark, N. Foster, C. M. Mason, M. K. Bennett, N. L. Simmons, and B. H. Hirst. 1996. Targeting to intestinal M cells. *J. Anat.* 189: 507–516.
17. Clark, M. A., M. A. Jepson, and B. H. Hirst. 1995. Lectin binding defines and differentiates M-cells in mouse small intestine and caecum. *Histochem. Cell Biol.* 104: 161–168.
18. Jepson, M. A., C. M. Mason, M. A. Clark, N. L. Simmons, and B. H. Hirst. 1995. Variations in lectin binding properties of intestinal M cells. *J. Drug Target* 3: 75–77.
19. Clark, M. A., M. A. Jepson, N. L. Simmons, T. A. Booth, and B. H. Hirst. 1993. Differential expression of lectin-binding sites defines mouse intestinal M-cells. *J. Histochem. Cytochem.* 41: 1679–1687.
20. Clark, M. A., M. A. Jepson, N. L. Simmons, and B. H. Hirst. 1995. Selective binding and transcytosis of *Ulex europaeus 1* lectin by mouse Peyer's patch M-cells in vivo. *Cell Tissue Res.* 282: 455–461.
21. Giannasca, P. J., K. T. Giannasca, P. Falk, J. I. Gordon, and M. R. Neutra. 1994. Regional differences in glycoconjugates of intestinal M cells in mice: potential targets for mucosal vaccines. *Am. J. Physiol.* 267: G1108–G1121.
22. Gebert, A., and W. Posselt. 1997. Glycoconjugate expression defines the origin and differentiation pathway of intestinal M-cells. *J. Histochem. Cytochem.* 45: 1341–1350.
23. Manocha, M., P. C. Pal, K. T. Chitralekha, B. E. Thomas, V. Tripathi, S. D. Gupta, R. Paranjape, S. Kulkarni, and D. N. Rao. 2005. Enhanced mucosal and systemic immune response with intranasal immunization of mice with HIV peptides entrapped in PLG microparticles in combination with *Ulex europaeus-I* lectin as M cell target. *Vaccine* 23: 5599–5617.
24. Wang, X., I. Kochetkova, A. Haddad, T. Hoyt, D. M. Hone, and D. W. Pascual. 2005. Transgene vaccination using *Ulex europaeus agglutinin I* (UEA-1) for targeted mucosal immunization against HIV-1 envelope. *Vaccine* 23: 3836–3842.

25. Wu, Y., X. Wang, K. L. Csencsits, A. Haddad, N. Walters, and D. W. Pascual. 2001. M cell-targeted DNA vaccination. *Proc. Natl. Acad. Sci. USA* 98: 9318–9323.
26. Lambkin, I., C. Pinilla, C. Hamashin, L. Spindler, S. Russell, A. Schink, R. Moya-Castro, G. Allicotti, L. Higgins, M. Smith, et al. 2003. Toward targeted oral vaccine delivery systems: selection of lectin mimetics from combinatorial libraries. *Pharm. Res.* 20: 1258–1266.
27. Takahashi, Y., S. Misumi, A. Muneoka, M. Masuyama, H. Tokado, K. Fukuzaki, N. Takamune, and S. Shoji. 2008. Nonhuman primate intestinal villous M-like cells: an effective poliovirus entry site. *Biochem. Biophys. Res. Commun.* 368: 501–507.
28. Misumi, S., R. Nakajima, N. Takamune, and S. Shoji. 2001. A cyclic dodecapeptide-multiple-antigen peptide conjugate from the undecapeptidyl arch (from Arg^{168} to Cys^{178}) of extracellular loop 2 in CCR5 as a novel human immunodeficiency virus type 1 vaccine. *J. Virol.* 75: 11614–11620.
29. Misumi, S., D. Nakayama, M. Kusaba, T. Iiboshi, R. Mukai, K. Tachibana, T. Nakasone, M. Umeda, H. Shibata, M. Endo, et al. 2006. Effects of immunization with CCR5-based cycloimmunogen on simian/HIVSF162P3 challenge. *J. Immunol.* 176: 463–471.
30. Gibellini, D., F. Vitone, E. Gori, M. La Placa, and M. C. Re. 2004. Quantitative detection of human immunodeficiency virus type 1 (HIV-1) viral load by SYBR green real-time RT-PCR technique in HIV-1 seropositive patients. *J. Virol. Methods* 115: 183–189.
31. Ui, M., T. Kuwata, T. Igarashi, K. Ibuki, Y. Miyazaki, I. L. Kozyrev, Y. Enose, T. Shimada, H. Uesaka, H. Yamamoto, et al. 1999. Protection of macaques against a SHIV with a homologous HIV-1 Env and a pathogenic SHIV-89.6P with a heterologous Env by vaccination with multiple gene-deleted SHIVs. *Virology* 265: 252–263.
32. Kernéis, S., A. Bogdanova, J. P. Kraehenbuhl, and E. Pringault. 1997. Conversion by Peyer's patch lymphocytes of human enterocytes into M cells that transport bacteria. *Science* 277: 949–952.
33. Clark, M. A., H. Blair, L. Liang, R. N. Brey, D. Brayden, and B. H. Hirst. 2001. Targeting polymerized liposome vaccine carriers to intestinal M cells. *Vaccine* 20: 208–217.
34. Hamashin, C., L. Spindler, S. Russell, A. Schink, I. Lambkin, D. O'Mahony, R. Houghten, and C. Pinilla. 2003. Identification of novel small-molecule *Ulex europaeus I* mimetics for targeted drug delivery. *Bioorg. Med. Chem.* 11: 4991–4997.
35. Veazey, R. S., M. Rosenzweig, D. E. Shvetz, D. R. Pauley, M. DeMaria, L. V. Chalifoux, R. P. Johnson, and A. A. Lackner. 1997. Characterization of gut-associated lymphoid tissue (GALT) of normal rhesus macaques. *Clin. Immunol. Immunopathol.* 82: 230–242.
36. Dustin, M. L., R. Rothlein, A. K. Bhan, C. A. Dinarello, and T. A. Springer. 1986. Induction by IL 1 and interferon-γ: tissue distribution, biochemistry, and function of a natural adherence molecule (ICAM-1). *J. Immunol.* 137: 245–254.
37. Koopman, G., H. K. Parmentier, H. J. Schuurman, W. Newman, C. J. Meijer, and S. T. Pals. 1991. Adhesion of human B cells to follicular dendritic cells involves both the lymphocyte function-associated antigen 1/intercellular adhesion molecule 1 and very late antigen 4/vascular cell adhesion molecule 1 pathways. *J. Exp. Med.* 173: 1297–1304.
38. Terahara, K., M. Yoshida, O. Igarashi, T. Nochi, G. S. Pontes, K. Hase, H. Ohno, S. Kurokawa, M. Mejima, N. Takayama, et al. 2008. Comprehensive gene expression profiling of Peyer's patch M cells, villous M-like cells, and intestinal epithelial cells. *J. Immunol.* 180: 7840–7846.
39. Sicinski, P., J. Rowinski, J. B. Warchol, Z. Jarzabek, W. Gut, B. Szczygiel, K. Bielecki, and G. Koch. 1990. Poliovirus type 1 enters the human host through intestinal M cells. *Gastroenterology* 98: 56–58.
40. Misumi, S., A. Eto, R. Mitsumata, M. Yamada, N. Takamune, and S. Shoji. 2008. Development of cell-expressed and virion-incorporated CCR5-targeted vaccine. *Biochem. Biophys. Res. Commun.* 377: 617–621.
41. Ohno, H., K. Hase, and K. Kawano. 2008. Antigen recognition, uptake and receptor on M cells. *Clin. Immunol. Allergol.* 19: 1–9.
42. Ueki, T., M. Mizuno, T. Uesu, T. Kiso, and T. Tsuji. 1995. Expression of ICAM-I on M cells covering isolated lymphoid follicles of the human colon. *Acta Med. Okayama* 49: 145–151.
43. Gullberg, E., A. V. Keita, S. Y. Salim, M. Andersson, K. D. Caldwell, J. D. Soderholm, and P. Artursson. 2006. Identification of cell adhesion molecules in the human follicle-associated epithelium that improve nanoparticle uptake into the Peyer's patches. *J. Pharmacol. Exp. Ther.* 319: 632–639.
44. Beyrer, C., A. W. Artenstein, S. Rugpao, H. Stephens, T. C. VanCott, M. L. Robb, M. Rinkaew, D. L. Birx, C. Khamboonruang, P. A. Zimmerman, et al. 1999. Epidemiologic and biologic characterization of a cohort of human immunodeficiency virus type 1 highly exposed, persistently seronegative female sex workers in northern Thailand: Chiang Mai HEPS Working Group. *J. Infect. Dis.* 179: 59–67.
45. Mazzoli, S., D. Trabattoni, S. Lo Caputo, S. Piconi, C. Ble, F. Meacci, S. Ruzzante, A. Salvi, F. Semplici, R. Longhi, et al. 1997. HIV-specific mucosal and cellular immunity in HIV-seronegative partners of HIV-seropositive individuals. *Nat. Med.* 3: 1250–1257.
46. Kaul, R., D. Trabattoni, J. J. Bwayo, D. Arienti, A. Zagliani, F. M. Mwangi, C. Kariuki, E. N. Ngugi, K. S. MacDonald, T. B. Ball, et al. 1999. HIV-1-specific mucosal IgA in a cohort of HIV-1-resistant Kenyan sex workers. *AIDS* 13: 23–29.
47. Barassi, C., A. Lazzarin, and L. Lopalco. 2004. CCR5-specific mucosal IgA in saliva and genital fluids of HIV-exposed seronegative subjects. *Blood* 104: 2205–2206.
48. Dean, M., M. Carrington, C. Winkler, G. A. Huttley, M. W. Smith, R. Allikmets, J. J. Goedert, S. P. Buchbinder, E. Vittinghoff, E. Gomperts, et al. 1996. Genetic restriction of HIV-1 infection and progression to AIDS by a deletion allele of the CKR5 structural gene: Hemophilia Growth and Development Study, Multicenter AIDS Cohort Study, Multicenter Hemophilia Cohort Study, San Francisco City Cohort, ALIVE Study. *Science* 273: 1856–1862.
49. Liu, R., W. A. Paxton, S. Choe, D. Ceradini, S. R. Martin, R. Horuk, M. E. MacDonald, H. Stuhlmann, R. A. Koup, and N. R. Landau. 1996. Homozygous defect in HIV-1 coreceptor accounts for resistance of some multiply-exposed individuals to HIV-1 infection. *Cell* 86: 367–377.
50. Samson, M., F. Libert, B. J. Doranz, J. Rucker, C. Liesnard, C. M. Farber, S. Saragosti, C. Lapoumeroulie, J. Cognaux, C. Forceille, et al. 1996. Resistance to HIV-1 infection in Caucasian individuals bearing mutant alleles of the CCR-5 chemokine receptor gene. *Nature* 382: 722–725.
51. Pastori, C., B. Weiser, C. Barassi, C. Uberti-Foppa, S. Ghezzi, R. Longhi, G. Calori, H. Burger, K. Kemal, G. Poli, et al. 2006. Long-lasting CCR5 internalization by antibodies in a subset of long-term nonprogressors: a possible protective effect against disease progression. *Blood* 107: 4825–4833.
52. Roth-Walter, F., I. Scholl, E. Untersmayr, R. Fuchs, G. Boltz-Nitulescu, A. Weissenbock, O. Scheiner, F. Gabor, and E. Jensen-Jarolim. 2004. M cell targeting with *Aleuria aurantia* lectin as a novel approach for oral allergen immunotherapy. *J. Allergy Clin. Immunol.* 114: 1362–1368.
53. Foster, N., M. A. Clark, M. A. Jepson, and B. H. Hirst. 1998. *Ulex europaeus 1* lectin targets microspheres to mouse Peyer's patch M-cells in vivo. *Vaccine* 16: 536–541.
54. Giannasca, P. J., K. T. Giannasca, A. M. Leichtner, and M. R. Neutra. 1999. Human intestinal M cells display the sialyl Lewis A antigen. *Infect. Immun.* 67: 946–953.
55. Sharma, R., E. J. van Damme, W. J. Peumans, P. Sarsfield, and U. Schumacher. 1996. Lectin binding reveals divergent carbohydrate expression in human and mouse Peyer's patches. *Histochem. Cell Biol.* 105: 459–465.

DOI: 10.1002/cmdc.201100542

A Synthetic C34 Trimer of HIV-1 gp41 Shows Significant Increase in Inhibition Potency

Wataru Nomura,[a] Chie Hashimoto,[a] Aki Ohya,[a] Kosuke Miyauchi,[b] Emiko Urano,[b] Tomohiro Tanaka,[a] Tetsuo Narumi,[a] Toru Nakahara,[a] Jun A. Komano,[b] Naoki Yamamoto,[c] and Hirokazu Tamamura*[a]

The development of new anti-HIV-1 drugs such as inhibitors of protease and integrase has been contributed to highly active anti-retroviral therapy (HAART) for the treatment of AIDS.[1] The entry of human immunodeficiency virus type 1 (HIV-1) into target cells is mediated by its envelope glycoprotein (Env), a type I transmembrane protein that consists of surface subunit gp120 and noncovalently associated transmembrane subunit gp41.[2] Sequential binding of HIV-1 gp120 to its cell receptor CD4 and a co-receptor (CCR5 or CXCR4) can trigger a series of conformational rearrangements in gp41 to mediate fusion between viral and cellular membranes.[3–5] The protein gp41 is hidden beneath gp120, and its ectodomain contains helical N- and C-terminal leucine/isoleucine heptad repeat domains, N-HR and C-HR. Particular regions of N-HR and C-HR are involved in membrane fusion, and 36-mer and 34-mer peptides, which are derived from N-HR and C-HR, have been designated as the N-terminal helix (N36) and C-terminal helix (C34), respectively. In the membrane fusion of HIV-1, these helices assemble to form a six-helical bundle (6-HB) consisting of a central parallel trimer of N36 surrounded by C34 in an antiparallel hairpin fashion. Synthetic peptides derived from these helices have potent antiviral activity against both laboratory-adapted strains and primary isolates of HIV-1.[6–9] They inhibit the membrane fusion stage of HIV-1 infection in a dominant-negative manner by binding to the counterpart regions of gp41 (N-HR or C-HR), blocking formation of the viral gp41 core.

Several potent anti-HIV-1 peptides based on the C-HR region have been discovered,[7,8] and T20 was subsequently developed as the clinical anti-HIV-1 drug enfuvirtide (Roche/Trimeris).[8,10–13] It is a 36-mer peptide derived from the gp41 C-HR sequence and can bind to the N-HR to prevent formation of the 6-HB in a dominant-negative fashion.[10] T20 therapy has brought safety, potent antiretroviral activity, and immunological benefit to patients, but its clinical application is limited by the development of resistance. The C-terminal helix C34 is also a C-HR-derived peptide, and contains the amino acid residues required for docking into the hydrophobic pocket, termed the "deep pocket", of the trimer of the N-HR region. This peptide potently inhibits HIV-1 fusion in vitro.[14] To date, several gp41 mimetics, especially those of N36 regions, which assemble these helical peptides with branched peptide linkers, have been synthesized as antigens.[15–19]

Recently, by using a novel template with C3-symmetric linkers of equal length, we synthesized a three-helix bundle mimetic that corresponds to the trimeric form of N36.[20] The antisera obtained from mice immunized by the peptide antigen showed strong recognition against the N36 trimer peptide with structural preference. At the same time, the trimer peptide was also investigated as a fusion inhibitor. However, the trimer N36 showed only a threefold increase in inhibition of HIV-1 fusion relative to the N36 monomer.[20] In terms of N36 content, the trimer and monomer have nearly the same inhibitory potency. This phenomenon is consistent with the results from other studies.[21–23] The multimerization of the functional unit, such as synthetic ligands against receptors, show synergistic binding and strong binding activity. Thus, we hypothesized that our strategy using C3-symmetric linkers in the design of trimer mimics of gp41 could be applied to the C34 peptide, which shows significant inhibition potency in the monomeric form. In the present study, we designed and synthesized a novel three-helical bundle structure of the trimeric form of C34. This equivalent mimic of the trimeric form of C34 was evaluated as a novel form of fusion inhibitor.

The C-terminal region of gp41 is known to be an assembly site involving a trimeric coiled-coil conformation. In the design of the C34-derived peptides C34REG-thioester (Figure 1 A) and C34REG (Figure 1 B), the triplet repeat of arginine and glutamic acid (RERERE) was added to the C-terminal end of the C34 sequence (residues 628–661) to increase aqueous solubility, and for C34REG-thioester, a glycine thioester was fused to the C terminus. To form a triple helix corresponding precisely to the gp41 pre-fusion form, we designed the novel C3-symmetric template depicted in Figure 1 C. This designed template linker has three branches of equal length, a hydrophilic structure, and a ligation site for coupling with C34REG-thioester. The template was synthesized as shown in Scheme 1. This approach uses native chemical ligation for chemoselective coupling of unprotected C34REG-thioester with a three-armed cysteine scaffold to produce triC34e (Figure 2).[24,25]

Circular dichroism (CD) spectra of C34REG and triC34e are shown in Figure 3 A. The peptides were dissolved in 50 mM sodium phosphate buffer with 150 mM NaCl, pH 7.2. Both spectra display minima at ~200 nm, indicating that these peptides form random structures. We previously reported that the

[a] Dr. W. Nomura, C. Hashimoto, A. Ohya, Dr. T. Tanaka, Dr. T. Narumi, T. Nakahara, Prof. Dr. H. Tamamura
Institute of Biomaterials and Bioengineering
Tokyo Medical and Dental University
2-3-10 Kandasurugadai, Chiyoda-ku, Tokyo 101-0062 (Japan)
E-mail: tamamura.mr@tmd.ac.jp

[b] Dr. K. Miyauchi, Dr. E. Urano, Dr. J. A. Komano
AIDS Research Center, National Institute of Infectious Diseases
1-23-1 Toyama, Shinjuku-ku, Tokyo 162-8640 (Japan)

[c] Prof. Dr. N. Yamamoto
Department of Microbiology, Yong Loo Lin School of Medicine
National University of Singapore
5 Science Drive 2, Singapore 117597 (Singapore)

Supporting information for this article is available on the WWW under http://dx.doi.org/10.1002/cmdc.201100542.

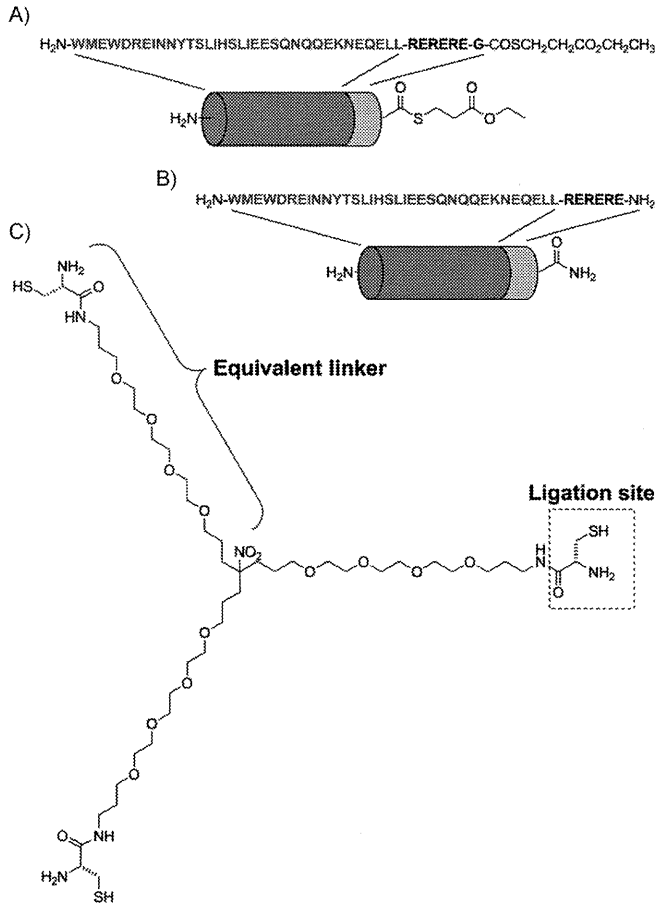

Figure 1. C34-derived peptides: A) C34REG-thioester and B) C34REG. C) The design of a C3-symmetric template.

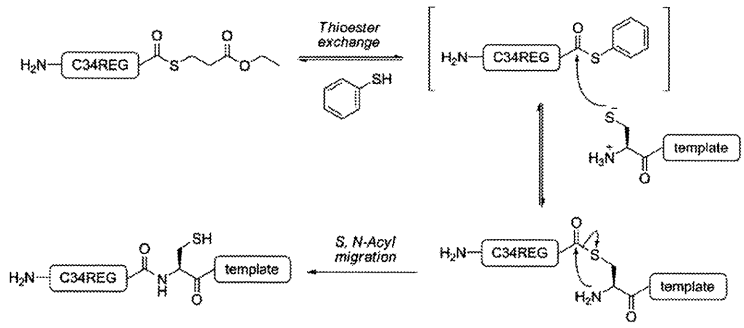

Figure 2. The native chemical ligation used for assembly of the C34REG-thioester on the template.

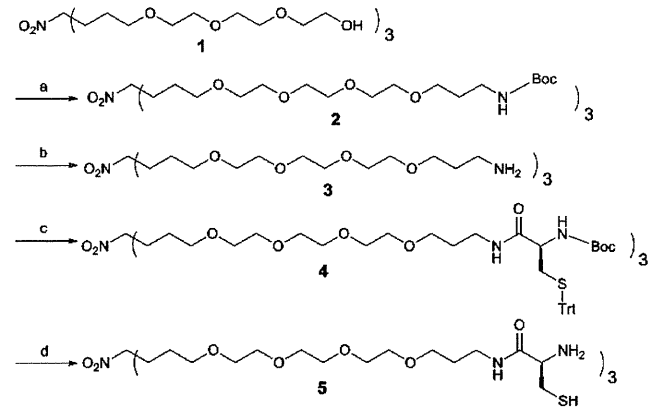

Scheme 1. Synthesis of the equivalently branched template **5**. *Reagents and conditions*: a) (3-bromopropyl)carbamic acid *tert*-butyl ester, NaH, THF; b) 4 M HCl/dioxane; c) Boc-Cys(Trt)-OH, EDCI·HCl, HOBt·H_2O, Et_3N, DMF; d) 90% aq. TFA.

helical content of the trimer triC34e and N36RE mixture is lower than that of the monomer C34REG and N36RE mixture. This is evidence that relative to the monomer C34REG, the trimer triC34e interacts with N36 only with difficulty, due to the assembly of three peptide strands by covalent bonds.

As the trimeric C34 was proven to interact with N36 helices, the potential HIV-1 inhibitory activities of the C-terminal peptides, C34REG and triC34e, were evaluated. The C34 peptide without the solubility-increasing sequence (3×[Arg-Glu], obtained from NIAID) was used as the monomeric control.[27] All peptides showed potent inhibitory activity in the viral fusion assay (Table 1), with the potency of triC34e being 100- and 40-fold higher than that of C34REG and C34 peptides, respectively. Notably, the triC34e trimer peptide is remarkably more potent in anti-HIV-1 activity than the monomer, indicating that a trimeric form is critical for inhibitory activity. Cytotoxicity from the peptides was not observed at concentrations of 15 μM for C34REG and C34, and 5 μM for triC34e.

We next carried out an assay for the inhibition of viral replication. As shown in Table 2, triC34e showed 30- and 20-fold higher inhibitory activity than peptides C34 and C34REG, respectively. In the two anti-HIV-1 assays, triC34e showed a great enhancement of activity over the C34 monomers. The IC_{50} values obtained in the assays are different, and this can be

N36 monomer N36RE and the N36 trimer triN36e form a highly structured α helix, and that the helical content of triN36e was greater than that of N36RE.[20,26] These results suggest that in contrast to N36-derived peptides, C34-derived peptides tend to form random structures both in the monomeric and trimeric forms. To assess the interaction of triC34e with N36, CD spectra of a mixture of triC34e with an N36-derived peptide, N36RE, were measured (Figure 3 B). The spectrum of the C34REG and N36RE mixture and that of the triC34e and N36RE mixture showed double minima at λ 208 and 222 nm, indicating that the peptide mixture forms an α-helical structure and that the

Table 1. IC_{50} and CC_{50} values determined by viral fusion inhibition and cell viability assays.

	C34 peptide[a]	C34REG	triC34e
IC_{50} [μM][b]	0.044	0.12	0.0013
CC_{50} [μM][c]	>15	>15	>5

[a] HIV-1 IIIB C34 peptide. [b] IC_{50} values are based on luciferase signals in TZM-bl cells infected with HIV-1 (NL4-3 strain). [c] CC_{50} values are based on the decrease in viability of TZM-bl cells. All data are the mean values from at least three experiments.

Table 2. IC_{50} values determined by inhibition assay based on p24 ELISA.			
	C34 peptide	C34REG	triC34e
IC_{50} [μM][a]	1.59	1.06	0.0547

[a] IC_{50} values are based on the production of p24 in MT-4 cells infected with HIV-1 (NL4-3 strain). All data are the mean values from at least three experiments.

explained through differences in experimental procedures. In the fusion inhibition assay, cells were treated with peptides before viral infection. In contrast, in the viral replication inhibition assay, peptides were treated after viral adsorption to cells. Therefore, in the latter case, the infection by HIV-1 might precede peptide binding to gp41.

It has been shown that T-1249, an analogue of enfuvirtide, and its hydrophobic C-terminal region inhibit HIV-1 fusion by interacting with lipid bilayers.[28] The tryptophan-rich domain of T-1249 was shown to play important roles in HIV-1 fusion.[29–31] As enfuvirtide shows weak interaction with the gp41 core structure, and the C34 sequence lacks the C-terminal lipid binding domain, it has been suggested that C34 has a mechanism of action distinct from that of enfuvirtide.[32] Thus, it is of interest to discern the mechanism of the enhanced inhibition observed with triC34e relative to the monomer. Two explanations can be envisaged: 1) the α helicity of the C34 trimer is higher than that of the monomer, as shown in Figure 3A, and as a result, the C34 trimer binds more strongly to the N36 trimer; and 2) in the mixture with the N36 monomer, the C34 trimer shows less α helicity than its monomer (Figure 3B). As shown in Figure 3A, the molar ellipticity at 222 nm is similar for both the C34 trimer and the monomer. Thus, the decrease at 222 nm in the mixture with N36 might be due to a decrease in the α helicity of N36. These results suggest that the C34 trimer might destabilize helix formation in N36 and thus exert potent inhibitory activity. It has been shown that a dimeric C37 (residues 625–661) variant does not show a significant difference in IC_{50} value against HIV-1 from wild-type C37, although the dimeric peptide shows tighter binding to the gp41 N-HR coiled-coil than the C37 monomer.[33] Thus, the mechanism of action of the C34 trimer could be different from that of the dimeric C-peptide. The detailed action mechanism of the trimer as a fusion inhibitor and the reasons behind its remarkable increased anti-HIV-1 activity will be the subjects of future studies in our research group.

A C-terminal helical peptide of HIV-1 gp41 has been designed as a new HIV fusion inhibitor and was synthesized with a novel template and three branched linkers of equal length. The native chemical ligation proceeded by chemoselective coupling in an aqueous medium of an unprotected C34 derivative containing a C-terminal thioester with a three-cysteine-armed scaffold. This process led to the production of triC34e. As a fusion inhibitor, triC34e has potent anti-HIV-1 activity, 100-fold greater than that of the C34REG monomer, although the anti-HIV-1 activity of the N36 trimer is threefold higher than that of the N36 monomer, and the N36 content is the same in both cases.[20] A trimeric form of C34 is evidently critical as the active structure of the fusion inhibitor. The soluble C34 derivative, SC34, retains potent inhibitory effects against enfuvirtide-resistant viruses,[34] and this suggests that the present highly potent trimeric inhibitor could be effective for enfuvirtide-resistant HIV-1 strains. The design of inhibitors that target the dynamic supramolecular mechanism of HIV-1 fusion will be useful for future studies of anti-HIV-1 agents.

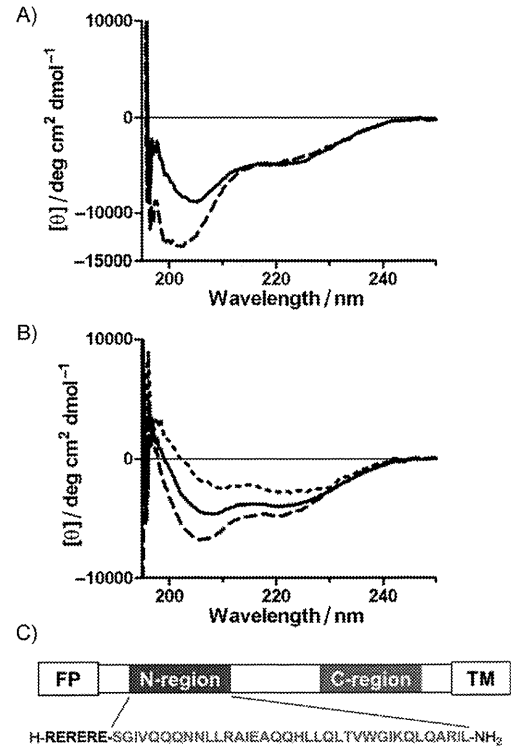

Figure 3. A) CD spectra of C34REG (monomer, -----, 6 μM) and triC34e (trimer, ——, 2 μM). B) CD spectra in the presence or absence of the N36 monomer N36RE:[20] -----, [C34REG (6 μM) + N36RE (6 μM)]; ——, [triC34e (2 μM) + N36RE (6 μM)]; ••••, N36RE (6 μM). In the amino acid sequence of N36RE, the triplet repeat of arginine and glutamic acid is located at the N-terminus of the original N36 sequence.[20] C) Amino acid sequence of N36RE: FP and TM represent the hydrophobic fusion peptide and transmembrane domains, respectively.

Experimental Section

Conjugation of C34REG-thioester and the template to produce triC34e

TCEP·HCl (773 μg, 2.67 μmol) and thiophenol (9 μL, 89 μmol) were dissolved in 0.1 M sodium phosphate buffer (60 μL) containing 6 M urea and EDTA (pH 8.5, 2 mM) under a nitrogen atmosphere. Compound **5** (100 μg, 0.0899 μmol), C34REG-thioester (1.77 mg, 0.297 μmol), and CH_3CN (20 μL) were added. The reaction was stirred for 5 h at 37 °C and monitored by HPLC. The ligation product (triC34e) was separated as an HPLC peak and characterized by ESI-ToF-MS (*m/z* calcd for $C_{703}H_{1108}N_{205}O_{245}S_6$ $[M+H]^+$: 16533.9, found: 16543.8). Purification was performed by reversed-phase HPLC (Cosmosil 5C_{18}-AR II column, 10×250 mm, Nacalai Tesque, Inc.) with elution using a 33–43% linear gradient of CH_3CN (0.1% TFA) over 40 min. Purified triC34e, obtained in 17% yield, was identified by ESI-ToF-MS. Details of the synthesis of these peptides are described in the Supporting Information.

CD spectra

Circular dichroism measurements were performed with a J-720 CD spectropolarimeter equipped with a thermoregulator (Jasco). The wavelength dependence of molar ellipticity [θ] was monitored at 25 °C from λ 195 to 250 nm. The peptides were dissolved in PBS (50 mM sodium phosphate, 150 mM NaCl, pH 7.2).

Virus preparation

For virus preparation, 293FT cells in a 60 mm dish were transfected with the pNL4-3 construct (10 μg) by the calcium phosphate method. The supernatant was collected 48 h after transfection, passed through a 0.45 μm filter, and stored at −80 °C as the virus stock.

Anti-HIV-1 assay

For the viral fusion inhibition assay, TZM-bl cells (2×10^4 cells per 100 μL) were cultured with the NL4-3 virus (5 ng of p24) and serially diluted peptides. After culture for 48 h, cells were lysed, and the luciferase activity was determined with the Steady-Glo luciferase assay system (Promega, Fitchburg, WI, USA).[35] For the viral replication inhibition assay, MT-4 cells (5×10^4 cells) were exposed to HIV-1 NL4-3 (1 ng of p24) at 4 °C for 30 min. After centrifugation, cells were resuspended with 150 μL medium containing indicated concentrations of serially diluted peptides. Cells were cultured at 37 °C for 3 days, and the concentration of p24 in the culture supernatant was determined by HIV-1 p24 antigen ELISA kit (ZeptoMetrix, Buffalo, NY, USA).

Cytotoxicity assay

The cytotoxic effects of peptides were determined by the CellTiter 96 AQueous One Solution Cell Proliferation assay system (Promega) under the same conditions, but in the absence of viral infection.

Acknowledgements

The following reagent was obtained through the US National Institutes of Health (NIH) AIDS Research and Reference Reagent Program, Division of AIDS, NIAID, NIH: HIV-1 IIIB C34 Peptide from DAIDS, NIAID. This work was supported in part by a Grant-in-Aid for Scientific Research from the Ministry of Education, Culture, Sports, Science, and Technology of Japan, and Health and Labour Sciences Research Grants from the Japanese Ministry of Health, Labor, and Welfare. C.H. is supported by JSPS research fellowships for young scientists.

Keywords: antiviral agents · C34 trimers · fusion inhibitors · gp41 · HIV-1

[1] C. Hashimoto, T. Tanaka, T. Narumi, W. Nomura, H. Tamamura, *Expert Opin. Drug Discovery* **2011**, *6*, 1067–1090.
[2] E. O. Freed, M. A. Martin, *J. Biol. Chem.* **1995**, *270*, 23883–23886.
[3] D. M. Eckert, P. S. Kim, *Annu. Rev. Biochem.* **2001**, *70*, 777–810.
[4] R. Wyatt, J. Sodroski, *Science* **1998**, *280*, 1884–1888.
[5] E. A. Berger, P. M. Murphy, J. M. Farber, *Annu. Rev. Immunol.* **1999**, *17*, 657–700.
[6] M. Lu, S. C. Blacklow, P. S. Kim, *Nat. Struct. Biol.* **1995**, *2*, 1075–1082.
[7] S. Jiang, K. Lin, N. Strick, A. R. Neurath, *Nature* **1993**, *365*, 113.
[8] C. T. Wild, D. C. Shugars, T. K. Greenwell, C. B. McDanal, T. J. Matthews, *Proc. Natl. Acad. Sci. USA* **1994**, *91*, 9770–9774.
[9] C. T. Wild, T. Oas, C. McDanal, D. Bolognesi, T. Matthews, *Proc. Natl. Acad. Sci. USA* **1992**, *89*, 10537–10541.
[10] J. M. Kilby, S. Hopkins, T. M. Venetta, B. DiMassimo, G. A. Cloud, J. Y. Lee, L. Alldredge, E. Hunter, D. Lambert, D. Bolognesi, T. Matthews, M. R. Johnson, M. A. Nowak, G. M. Shaw, M. S. Saag, *Nat. Med.* **1998**, *4*, 1302–1307.
[11] J. M. Kilby, J. J. Eron, *N. Engl. J. Med.* **2003**, *348*, 2228–2238.
[12] J. P. Lalezari, K. Henry, M. O'Hearn, J. S. Montaner, P. J. Piliero, B. Trottier, S. Walmsley, C. Cohen, D. R. Kuritzkes, J. J. Eron, Jr., J. Chung, R. DeMasi, L. Donatacci, C. Drobnes, J. Delehanty, M. Salgo, *N. Engl. J. Med.* **2003**, *348*, 2175–2185.
[13] S. Liu, W. Jing, B. Cheng, H. Lu, J. Sun, X. Yan, J. Niu, J. Farmar, S. Wu, S. Jiang, *J. Biol. Chem.* **2007**, *282*, 9612–9620.
[14] D. C. Chan, D. Fass, J. M. Berger, P. S. Kim, *Cell* **1997**, *89*, 263–273.
[15] E. De Rosny, R. Vassell, R. T. Wingfield, C. T. Wild, C. D. Weiss, *J. Virol.* **2001**, *75*, 8859–8863.
[16] J. P. Tam, Q. Yu, *Org. Lett.* **2002**, *4*, 4167–4170.
[17] W. Xu, J. W. Taylor, *Chem. Biol. Drug Des.* **2007**, *70*, 319–328.
[18] J. M. Louis, I. Nesheiwat, L. Chang, G. M. Clore, C. A. Bewlet, *J. Biol. Chem.* **2003**, *278*, 20278–20285.
[19] E. Bianch, J. G. Joyce, M. D. Miller, A. C. Finnefrock, X. Liang, M. Finotto, P. Ingllinella, P. McKenna, M. Citron, E. Ottinger, R. W. Hepler, R. Hrin, D. Nahas, C. Wu, D. Montefiori, J. W. Shiver, A. Pessi, P. S. Kim, *Proc. Natl. Acad. Sci. USA* **2010**, *107*, 10655–10660.
[20] T. Nakahara, W. Nomura, K. Ohba, A. Ohya, T. Tanaka, C. Hashimoto, T. Narumi, T. Murakami, N. Yamamoto, H. Tamamura, *Bioconjugate Chem.* **2010**, *21*, 709–714.
[21] M. Lu, H. Ji, S. Shen, *J. Virol.* **1999**, *73*, 4433–4438.
[22] D. M. Eckert, P. S. Kim, *Proc. Natl. Acad. Sci. USA* **2001**, *98*, 11187–11192.
[23] E. Bianchi, M. Finotto, P. Ingallinella, R. Hrin, A. V. Carella, X. S. Hous, W. A. Schleif, M. D. Miller, *Proc. Natl. Acad. Sci. USA* **2005**, *102*, 12903–12908.
[24] P. E. Dawson, T. W. Muir, I. Clark-Lewis, S. B. H. Kent, *Science* **1994**, *266*, 776–779.
[25] P. E. Dawson, M. J. Churchill, M. R. Ghadiri, S. B. H. Kent, *J. Am. Chem. Soc.* **1997**, *119*, 4325–4329.
[26] D. C. Chan, C. T. Chutkowski, P. S. Kim, *Proc. Natl. Acad. Sci. USA* **1998**, *95*, 15613–15617.
[27] S. A. Gallo, K. Sackett, S. S. Rawat, Y. Shai, R. Blumenthal, *J. Mol. Biol.* **2004**, *340*, 9–14.
[28] A. S. Veiga, N. C. Santos, L. M. Loura, A. Fedorov, M. A. Castanho, *J. Am. Chem. Soc.* **2004**, *126*, 14758–14763.
[29] M. K. Lawless, S. Barney, K. I. Guthrie, T. B. Bucy, S. R. Petteway, Jr., G. Merutka, *Biochemistry* **1996**, *35*, 13697–13708.
[30] K. Salzwedel, J. T. West, E. Hunter, *J. Virol.* **1999**, *73*, 2469–2480.
[31] S. G. Peisajovich, S. A. Gallo, R. Blumenthal, Y. Shai, *J. Biol. Chem.* **2003**, *278*, 21012–21017.
[32] S. Liu, H. Lu, Y. Xu, S. Wu, S. Jiang, *J. Biol. Chem.* **2005**, *280*, 11259–11273.
[33] K. M. Kahle, K. Steger, M. J. Root, *PLoS Pathog.* **2009**, *5*, e1000674.
[34] A. Otaka, M. Nakamura, D. Nameki, E. Kodama, S. Uchiyama, S. Nakamura, H. Nakano, H. Tamamura, Y. Kobayashi, M. Matsuoka, N. Fujii, *Angew. Chem.* **2002**, *114*, 3061–3064; *Angew. Chem. Int. Ed.* **2002**, *41*, 2937–2940.
[35] E. J. Platt, K. Wehrly, S. E. Kuhmann, B. Chesebro, D. Kabat, *J. Virol.* **1998**, *72*, 2855–2864.

Received: November 22, 2011
Revised: December 15, 2011
Published online on January 13, 2012

J|A|C|S
COMMUNICATIONS

Published on Web 10/25/2010

Bivalent Ligands of CXCR4 with Rigid Linkers for Elucidation of the Dimerization State in Cells

Tomohiro Tanaka, Wataru Nomura,* Tetsuo Narumi, Akemi Masuda, and Hirokazu Tamamura*

Department of Medicinal Chemistry, Institute of Biomaterials and Bioengineering, Tokyo Medical and Dental University, 2-3-10 Kandasurugadai, Chiyoda-ku, Tokyo 101-0062, Japan

Received August 18, 2010; E-mail: nomura.mr@tmd.ac.jp; tamamura.mr@tmd.ac.jp

Abstract: To date, challenges in the design of bivalent ligands for G protein-coupled receptors (GPCRs) have revealed difficulties stemming from lack of knowledge of the state of oligomerization of the GPCR. The synthetic bivalent ligands with rigid linkers that are presented here can predict the dimer form of CXCR4 and be applied to molecular probes in cancerous cells. This "molecular ruler" approach would be useful in elucidating the details of CXCR4 oligomer formation.

The chemokine receptor CXCR4 is a membrane protein belonging to the family of G protein-coupled receptors (GPCRs). In current drugs, ~60% of drug target molecules are located at the cell surface, and half of them are GPCRs.[1] Recent studies have indicated a pivotal role for homo- and heterooligomerization of CXCR4 in cancer metastasis, and the significance of oligomeric forms of GPCR has been gaining acceptance.[2] However, the functional implications proposed for these oligomers, which include signal transduction and internalization, are poorly understood and require additional studies.[3] Efforts to understand those correlations have used photochemical analyses such as bioluminescence resonance energy transfer (BRET) analysis,[3,4] but the elucidation of the native state of CXCR4 in living cells is complicated by conformational or functional changes resulting from mutations. Estimates of the precise distance between ligand binding sites in the dimer form would permit the development of bivalent ligands of CXCR4 having improved binding affinity and specificity.[5] In spite of the enormous effort devoted to the design of bivalent ligands, rational design of such linkers has been difficult because of the lack of knowledge concerning the dimeric form of GPCRs. Therefore, there is an increasing demand for a novel strategy for the analysis of the precise distance between ligand binding sites.[6]

In this study, we designed and synthesized novel CXCR4 bivalent ligands consisting of two molecules of an FC131[7] analogue, [*cyclo*(-D-Tyr-Arg-Arg-Nal-D-Cys-)] [Nal = L-3-(2-naphthyl)alanine, **1a**], connected by a poly(L-proline) or a PEGylated poly(L-proline) linker. Poly(L-prolines) have been utilized as rigid linkers between the two functional units, which require a predetermined separation for activity.[8] Linkers consisting of poly(L-prolines) were expected to maintain constant distances of 2−8 nm between the ligands. Our bivalent ligands with linkers of various lengths were used to determine the distance between two binding sites of ligands consisting of CXCR4 dimers. Acetamide-capped FC131 (**1b**), in which Gly is replaced by D-Cys and the thiol group of Cys is capped with an acetamide group, was synthesized as a monomer unit of the ligand (Figure 1). Although this substitution caused a 2-fold decrease in binding to CXCR4, the binding affinity was still adequate for analyses. Poly(L-proline) helices are known to maintain a length of 0.9 nm per turn.[9] In this study, polyproline- and

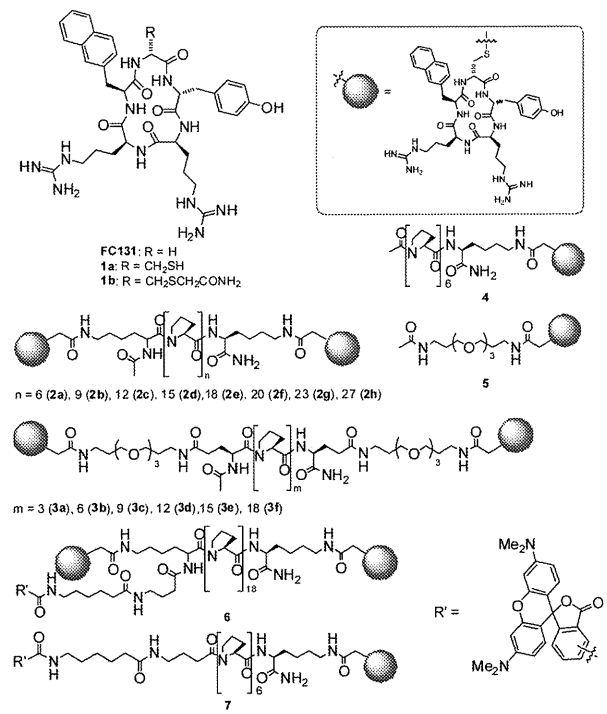

Figure 1. Design of bivalent ligands against chemokine receptor CXCR4. As CXCR4 binding moieties, D-Cys FC131 (R = CH_2SH, **1a**) and acetamide-capped FC131 (R = $CH_2SCH_2CONH_2$, **1b**) were prepared. Poly(L-proline) (**2a**−**h**) and PEG-conjugated poly(L-proline) (**3a**−**f**) with CXCR4 binding moieties on both ends were synthesized. As monomer binding ligands with linkers, Ac6pro FC131 (**4**) and AcPEG FC131 (**5**) were synthesized. Tetramethylrhodamine (TAMRA)-labeled **2e** (**6**) and **4** (**7**) were prepared for the imaging experiments.

PEGylated polyproline-type linkers with lengths of 2−8 nm were synthesized.[10] The synthetic linkers and their conjugated bivalent ligands were characterized by high-resolution mass spectrometry (HRMS) (Tables S3 and S5 in the Supporting Information), and their CD spectra clearly showed the presence of a type-II polyproline helix (Figure S3 in the Supporting Information). As monomer controls, FC131 analogues **4** and **5** with hexaproline and poly(ethylene glycol) (PEG) linkers, respectively, that were acetylated at the other end were also prepared.

The binding affinities of the synthetic ligands were evaluated in a competitive binding assay against [^{125}I]-SDF-1α, as reported previously.[7d] The binding assay showed that the binding affinity of our bivalent ligands is clearly dependent on the linker length. Ligands of the poly(L-proline) type with the highest affinities were **2e** and **2f**. Among the PEGylated poly(L-proline)-type ligands, **3c** and **3d** showed the highest affinity. The linker-optimized bivalent ligands, **2f** and **3d**, showed 7.3- and 21-fold increases in binding affinity relative to **4** and **5**, respectively (Table 1). These results

10.1021/ja107447w

Table 1. Summary of Binding Affinities of Synthetic Bivalent and Monovalent Ligands Analyzed by [^{125}I]-SDF-1α Competition Assay

compd	K_i (nM)[a]	linker length (nm)	compd	K_i (nM)[a]	linker length (nm)
FC131	31.5	–	**3a**	87.2	3.8
1b	53.4	–	**3b**	45.6	4.7
2a	51.2	1.8	**3c**	17.8	5.6
2b	45.4	2.7	**3d**	13.9	6.5
2c	64.4	3.6	**3e**	49.3	7.4
2d	59.5	4.5	**3f**	83.3	8.3
2e	13.2	5.4	**4**	72	–
2f	9.9	6	**5**	294	–
2g	22.5	6.9	**7**	119	–
2h	45.8	8.1			

[a] K_i values are the concentrations corresponding to 50% inhibition of [^{125}I]-SDF-1α binding to Jurkat cells.

indicate successful bivalent binding of the ligands, which has been known to be responsible for an increase in binding affinity.[5a] It should be noted that the maximum increase in binding affinity was observed for ligands of the two linker types having similar lengths (5.5–6.5 nm). In the dimer state of CXCR4, there are several forms of assembly (head-to-head, tail-to-tail, and head-to-tail).[5a] These forms have different distances between the binding sites of the ligands. Molecular modeling studies of FC131 with CXCR4 suggested that amino acids in transmembrane (TM) 7 are important for FC131 binding.[11] Through the use of the rhodopsin structure, it was revealed that in the TM 4 and 5 assembly form, the linear distance between ligand binding sites is 5.3 nm. In the other forms of possible assembly, the linear distances were determined to be 3.5 and 3.9 nm for TM 1 and 2 assembly and the combination of TM 1–4 and TM 2–5 assembly, respectively (Figure S4). The changes in binding affinity were relatively moderate, and although the existence of different assembly forms is possible, a majority of the population should be in the TM 4 and 5 assembly form.

From the increased binding affinity of linker-optimized bivalent ligands, a hypothesis was derived that such ligands could be applied as probes specific to CXCR4 on the cell surface because the receptors are overexpressed in several kinds of malignant cells[12] and that the dimer formation of the receptor should depend on the expression level. Accordingly, compound **2e**, which showed high binding affinity, was chosen for labeling with tetramethylrhodamine (TAMRA) and applied to the imaging of CXCR4. The TAMRA moiety was conjugated to an N-teminal of the proline linker via γ-butyric acid. To confirm that the ligands specifically bind to CXCR4, a CXCR4–EGFP fusion protein (EGFP = enhanced green fluorescent protein) was transiently expressed in HeLa cells. The increase in binding affinity of the bivalent ligand was clearly reflected in the imaging of CXCR4, as a merged image of TAMRA-labeled **2e** (**6**) and EGFP-fused CXCR4 was observed (Figure 2). When a control monomer, TAMRA-labeled **4** (**7**), was utilized for detection, only a trace of binding was observed. Additionally, binding to mock HeLa cells at the same concentration of ligands was not observed for either ligand (Figure S5).

To further evaluate the binding specificity and dependence on CXCR4 expression levels, fluorescence-activated cell sorting (FACS) analyses utilizing Jurkat, K562, and HeLa cells were performed (Figure 3). The cells were adopted on the basis of their different levels of CXCR4 expression (Jurkat > HeLa > K562).[13] The binding was evaluated by changes in mean fluorescence intensity (MFI) of the above cells in the presence and absence of ligands. The bivalent ligand **6** showed intense binding to Jurkat cells, which highly express CXCR4, as evidenced by the 2.3- and 3.3-fold increases in MFI at 25 and 250 nM, respectively. For binding to HeLa cells, the MFI was increased 2.4-fold by binding

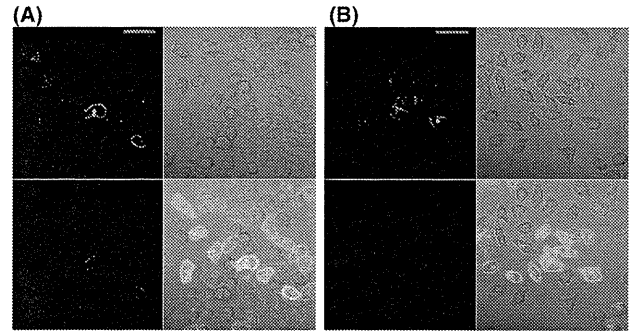

Figure 2. Binding of TAMRA-labeled FC131-derived monovalent and bivalent ligands to EGFP–CXCR4-transfected HeLa cells. Bivalent ligand **6** with an optimized linker length was utilized. The pictures show the binding of (A) **6** (25 nM) and (B) **7** (50 nM). Each panel is divided into four sections as follows: upper left, EGFP emission; upper right, differential interference contrast (DIC) image; lower left, TAMRA emission conjugated to ligands; lower right, merged image. Orange bars in the panels represent 50 μm.

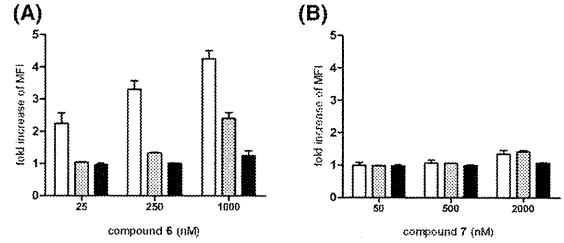

Figure 3. FACS analysis to evaluate the dependence of ligand binding on the levels of CXCR4 expression. The columns show the binding of (A) **6** and (B) **7** to Jurkat (white), HeLa (gray), and K562 (black) cells. The fold increase values were calculated by dividing the MFIs of the above cells in the presence of ligands by the corresponding values in the absence of ligands. The results are means of three independent experiments; error bars indicate standard errors of the mean.

of ligand **6** at 1 μM, although no significant increase in MFI was observed at 25 or 250 nM **6**, which corresponds with the imaging experiment (Figure S5). Meanwhile, the monovalent ligand **7** at 2 μM showed similar binding to Jurkat and HeLa cells, involving 1.1- and 1.4-fold increases in MFI, respectively. These results suggest that it is difficult to distinguish the expression level of CXCR4 by molecular imaging using the monovalent ligand. On the other hand, it is of special interest that the bivalent ligand showed distinguishability of the differences in CXCR4 expression levels. Furthermore, the binding of our CXCR4 ligands would be responsive to CXCR4, as no binding of either ligand to K562 cells, which express a trace of CXCR4, was observed. These results provide evidence in support of the hypothesis that the bivalent ligand binds preferentially to the constitutive dimer of CXCR4. Molecular imaging of CXCR4 on the cell surface by specific antibodies, such as c8352[14] or the monomer ligand T140,[15] has been previously reported. In the present system, however, it is possible that the bivalent ligands could distinguish the density of CXCR4 on the cell surface.

To further assess whether our bivalent ligand could distinguish between cancerous and normal cells by the imaging method, A549 and Human Umbilical Vein Endothelial Cells (HUVEC) were employed for staining as adhesive cell lines. A549 cells are human lung adenocarcinomic human alveolar basal epithelial cells, which are known to possess high CXCR4 expression levels.[16] HUVEC were chosen as a normal cell line without CXCR4 expression. It has been reported that the expression of CXCR4 on HUVEC is induced by fibroblast growth factor (FGF), which is highly expressed in the embryonic stage.[17] Thus, HUVEC was cultured

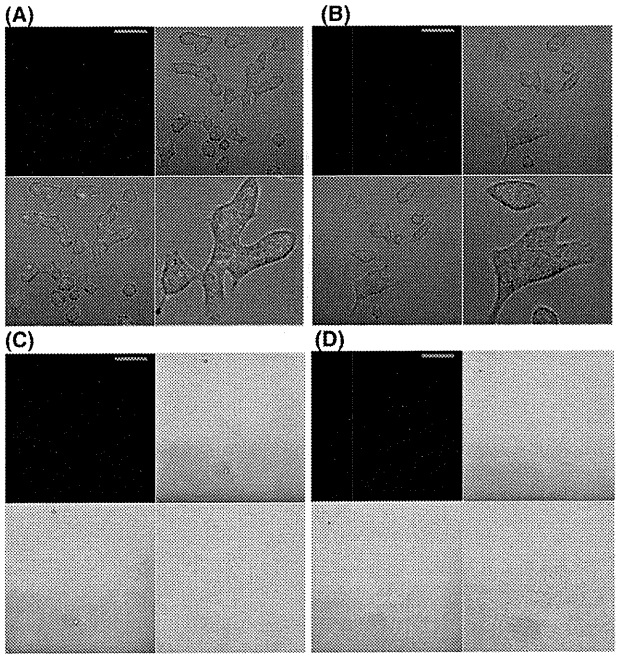

Figure 4. Imaging of CXCR4 by TAMRA-labeled FC131-derived monovalent and bivalent ligands on cancerous and normal primary cells. The panels show the binding of (A) **6** (1 μM) and (b) **7** (2 μM) to A549 cells and (C) **6** (250 nM) and (D) **7** (500 nM) to HUVEC cells. Each panel is divided into four sections as follows: upper left, TAMRA emission image; upper right; DIC image; lower left, merged image; lower right, focused image. Orange bars in the panels represent 50 μm.

in the absence of FGF. Ligand **6** showed clear binding to A549 cells (Figure 4A) but not to HUVEC (Figure 4C) at concentrations of 1 μM and 250 nM, respectively. On the other hand, monomer ligand **7** showed a trace of binding to each cell line (Figure 4B,D). Bivalent ligand **6** showed binding to HUVEC cultured with FGF at 250 nM (Figure S7). Thus, the bivalent ligands can detect cancerous cells that are in a state of high CXCR4 expression in a specific manner.

In summary, we have presented experimental results concerning the elucidation of the native state of the CXCR4 dimer utilizing bivalent ligands. These lead to a more precise understanding of the oligomerization state. Such a "molecular ruler" approach could be utilized in the design of bivalent ligands for any GPCR. It has been suggested that several GPCRs also exist as heterodimer forms, and CXCR4 has been hypothesized to form heterodimers with CCR2,[18] CCR5,[19] CXCR7,[4b] and the δ-opioid receptor.[20] Although the biological significance of GPCRs in homo- or heterooligomerization is still unclear and controversial, the approach described here involving rigid linkers conjugated to ligands specific to each GPCR would lead to elucidation of these issues. Furthermore, through the avidity shown as the specific binding affinity for the dimeric form of CXCR4, the fluorescent-labeled bivalent ligands have been shown to be powerful tools for cancer diagnosis on the basis of their ability to distinguish the density of CXCR4 on the cell surface. Our approach has the advantages that the ligand can directly capture dimeric forms of GPCRs and that the linkers can be applied to virtually any known GPCR.

Acknowledgment. The authors thank Prof. Kazunari Akiyoshi (Tokyo Medical and Dental University) for access to the laser scanning microscope. T.T. was supported by JSPS Research Fellowships for Young Scientists. This research was supported in part by New Energy and Industrial Technology Development Organization (NEDO).

Supporting Information Available: Curve-fitting data for the binding analyses, CD spectra, docking study of bivalent ligand binding, imaging analyses of mock cells, histogram and MFI of FACS analysis, imaging analyses of HeLa cells cultured with FGF, experimental procedures, and spectral and analytical data for all new compounds. This material is available free of charge via the Internet at http://pubs.acs.org.

References

(1) Overington, J. P.; Al-Lazikani, B.; Hopkins, A. L. *Nat. Rev. Drug. Discovery* **2006**, *5*, 993–996.
(2) Wang, J.; He, L.; Combs, C. A.; Roderiquez, G.; Norcross, M. A. *Mol. Cancer Ther.* **2006**, *5*, 2474–2483.
(3) Percherancier, Y.; Berchiche, Y. A.; Slight, I.; Volkmer-Engert, R.; Tamamura, H.; Fujii, N.; Bouvier, M.; Heveker, N. *J. Biol. Chem.* **2005**, *280*, 9895–9903.
(4) (a) Babcock, G. J.; Farzan, M.; Sodroski, J. *J. Biol. Chem.* **2003**, *278*, 3378–3385. (b) Luker, K. E.; Gupta, M.; Luker, G. D. *FASEB J.* **2009**, *23*, 823–834.
(5) (a) Handl, H. L.; Sankaranarayanan, R.; Josan, J. S.; Vagner, J.; Mash, E. A.; Gillies, R. J.; Hruby, V. J. *Bioconjugate Chem.* **2007**, *18*, 1101–1109. (b) Zheng, Y.; Akgün, E.; Harikumar, K. G.; Hopson, J.; Powers, M. D.; Lunzer, M. M.; Miller, L. J.; Portoghese, P. S. *J. Med. Chem.* **2009**, *52*, 247–258.
(6) Panetta, R.; Greenwood, M. T. *Drug Discovery Today* **2008**, *13*, 1059–1066.
(7) (a) Tamamura, H.; Xu, Y.; Hattori, T.; Zhang, X.; Arakaki, R.; Kanbara, K.; Omagari, A.; Otaka, A.; Ibuka, T.; Yamamoto, N.; Nakashima, H.; Fujii, N. *Biochem. Biophys. Res. Commun.* **1998**, *253*, 877–882. (b) Fujii, N.; Oishi, S.; Hiramatsu, K.; Araki, T.; Ueda, S.; Tamamura, H.; Otaka, A.; Kusano, S.; Terakubo, S.; Nakashima, H.; Broach, J. A.; Trent, J. O.; Wang, Z.; Peiper, S. C. *Angew. Chem., Int. Ed.* **2003**, *42*, 3251–3253. (c) Tamamura, H.; Araki, T.; Ueda, S.; Wang, Z.; Oishi, S.; Esaka, A.; Trent, J. O.; Nakashima, H.; Yamamoto, N.; Peiper, S. C.; Otaka, A.; Fujii, N. *J. Med. Chem.* **2005**, *48*, 3280–3289. (d) Tanaka, T.; Tsutsumi, H.; Nomura, W.; Tanabe, Y.; Ohashi, N.; Esaka, A.; Ochiai, C.; Sato, J.; Itotani, K.; Murakami, T.; Ohba, K.; Yamamoto, N.; Fujii, N.; Tamamura, H. *Org. Biomol. Chem.* **2008**, *6*, 4374–4377.
(8) (a) Arora, P. S.; Ansari, A. Z.; Best, T. P.; Ptashne, M.; Dervan, P. B. *J. Am. Chem. Soc.* **2002**, *124*, 13067–13071. (b) Sato, S.; Kwon, Y.; Kamisuki, S.; Srivastava, N.; Mao, Q.; Kawazoe, Y.; Uesugi, M. *J. Am. Chem. Soc.* **2007**, *129*, 873–880.
(9) (a) Kuemin, M.; Schweizer, S.; Ochsenfeld, C.; Wennemers, H. *J. Am. Chem. Soc.* **2009**, *131*, 15474–15482. (b) Schuler, B.; Lipman, E. A.; Steinbach, P. J.; Kumke, M.; Eaton, W. A. *Proc. Natl. Acad. Sci. U.S.A.* **2005**, *102*, 2754–2759.
(10) For synthesis details, see the Supporting Information.
(11) Våbenø, J.; Nikiforovich, G. V.; Marshall, G. R. *Chem. Biol. Drug Des.* **2006**, *67*, 346–354.
(12) Balkwill, F. *Semin. Cancer Biol.* **2004**, *14*, 171–178.
(13) (a) Carnec, X.; Quan, L.; Olson, W. C.; Hazan, U.; Dragic, T. *J. Virol.* **2005**, *79*, 1930–1933. (b) Majka, M.; Rozmyslowicz, T.; Honczarenko, M.; Ratajczak, J.; Wasik, M. A.; Gaulton, G. N.; Ratajczak, M. Z. *Leukemia* **2000**, *14*, 1821–1832.
(14) Schwartz, V.; Lue, H.; Kraemer, S.; Korbiel, J.; Krohn, R.; Ohl, K.; Bucala, R.; Weber, C.; Bernhagen, J. *FEBS Lett.* **2009**, *583*, 2749–2757.
(15) Nomura, W.; Tanabe, Y.; Tsutsumi, H.; Tanaka, T.; Ohba, K.; Yamamoto, N.; Tamamura, H. *Bioconjugate Chem.* **2008**, *19*, 1917–1920.
(16) Murdoch, C.; Monk, P. N.; Finn, A. *Immunology* **1999**, *98*, 36–41.
(17) Salcedo, R.; Wasserman, K.; Young, H. A.; Grimm, M. C.; Howard, O. M. Z.; Anver, M. R.; Kleinman, H. K.; Murphy, W. J.; Oppenheim, J. J. *Am. J. Pathol.* **1999**, *154*, 1125–1135.
(18) Sohy, D.; Parmentier, M.; Springael, J. *J. Biol. Chem.* **2007**, *282*, 30062–30069.
(19) Contento, R. L.; Molon, B.; Boularan, C.; Pozzan, T.; Manes, S.; Marullo, S.; Viola, A. *Proc. Natl. Acad. Sci. U.S.A.* **2008**, *105*, 10101–10106.
(20) Pello, O. M.; Martínez-Muñoz, L.; Parrillas, V.; Serrano, A.; Rodríguez-Frade, J. M.; Toro, M. J.; Lucas, P.; Monterrubiol, M.; Martínez-A, C.; Mellado, M. *Eur. J. Immunol.* **2008**, *38*, 537–549.

JA107447W

Remodeling of Dynamic Structures of HIV-1 Envelope Proteins Leads to Synthetic Antigen Molecules Inducing Neutralizing Antibodies

Toru Nakahara,[†] Wataru Nomura,*[,†] Kenji Ohba,[‡] Aki Ohya,[†] Tomohiro Tanaka,[†] Chie Hashimoto,[†] Tetsuo Narumi,[†] Tsutomu Murakami,[‡] Naoki Yamamoto,[‡] and Hirokazu Tamamura*[,†]

Department of Medicinal Chemistry, Institute of Biomaterials and Bioengineering, Tokyo Medical and Dental University, 2-3-10 Kandasurugadai, Chiyoda-ku, Tokyo 101-0062, Japan, and AIDS Research Center, National Institute of Infectious Diseases, 1-23-1 Toyama, Shinjuku-ku, Tokyo 162-8640, Japan. Received November 16, 2009; Revised Manuscript Received February 28, 2010

A synthetic antigen targeting membrane-fusion mechanism of HIV-1 has a newly designed template with C3-symmetric linkers mimicking N36 trimeric form. The antiserum produced by immunization of the N36 trimeric form antigen showed structural preference in binding to N36 trimer and stronger inhibitory activity against HIV-1 infection than the N36 monomer. Our results suggest an effective strategy of HIV vaccine design based on a relationship to the native structure of proteins involved in HIV fusion mechanisms.

INTRODUCTION

Antibody-based therapy is one of the promising treatments for AIDS. In recent years, AIDS antibodies have been produced by immunization (*1*) and by de novo engineering of monoclonal antibodies (mAb) with molecular evolution tactics such as phage display (*2*). Despite enormous efforts, however, only a limited number of highly and broadly HIV-neutralizing human mAbs have been isolated and characterized. These antibodies include gp41 Abs, 2F5 (*3*−*6*) and 4E10 (*5*−*7*), and gp120 Abs, 2G12 (*8*) and b12 (*9*). gp41 is a transmembrane envelope glycoprotein, which is divided into an endodomain and an ectodomain by the transmembrane region; the latter contains a hydrophobic amino-terminal fusion peptide, followed by amino-terminal and carboxy-terminal leucine/isoleucine heptad repeat domains with helical structures (HR1 and HR2, respectively). In the membrane fusion process of HIV-1, these subunits form a "pre-bundle" complex. The HR1 and HR2 regions are termed the N-terminal helix (N36) and C-terminal helix (C34), respectively. These helices form a six-helical bundle consisting of a central parallel trimeric coiled-coil of N36 surrounded by C34 in an antiparallel hairpin fashion. In design of immunogens that elicit broadly neutralizing antibodies, a useful strategy is to produce molecules that mimic the natural trimer on the virion surface. Previous studies show that these molecules could be proteins expressed as a recombinant form or on the surface of particles such as pseudovirions or proteoliposomes (*10*−*12*). The X-ray crystallographic study of gp41 shows that the distances between any two residues at the N-terminus of N-region are almost equal at approximately 10 Å (Figure 1A). A chemically synthetic template could be useful in connection with the design of a peptidomimetic corresponding to the native structure of gp41. To date, several gp41 mimetics have been synthesized as inhibitors or antigens and subjected to inhibition or neutralization assays (*13*−*16*). However, the templates for assembly of these helical peptides contain branched peptide linkers, which are not exactly equivalent in length (*14*). The N-terminal peptides constrained by another threefold linker showed high affinity for C-terminal peptides, although its biological advantages have not been determined (*15*). The mimicry can be estimated using the broadly neutralizing mAbs; suitable mimetics will bind neutralizing mAbs efficiently, but they will bind non-neutralizing mAbs poorly. In the present study, we designed and synthesized a novel three-helical bundle mimetic, which corresponds to the trimeric form of N36. We investigated whether mice immunized with the equivalent trimeric form of N36 mimetic can produce antibodies with stronger binding affinity for N36 trimer than for N36 monomer. This approach demonstrates the possibility of producing structure-specific antibodies by immunization of synthetic antigens corresponding to the natural form of viral proteins.

EXPERIMENTAL PROCEDURES

Conjugation of N36REGC and the Template to Produce triN36e. Compound **6** (100 μg, 0.174 μmol) and N36REGC (3.4 mg, 0.574 μmol) were dissolved in a mixture of 300 μL of 200 mM acetate buffer (pH 5.2) and 300 μL of TFE under a nitrogen atmosphere, then TCEP·HCl was added. The reaction was stirred for 72 h at room temperature and monitored by HPLC. The ligation product (triN36e) was separated as an HPLC peak and was characterized by ESI-TOF-MS, *m/z* calcd for $C_{690}H_{1160}N_{226}O_{201}S_3$ 15933.1, found 15933.8. The purification was performed by reverse phase HPLC (YMC-Pack ODS-A column, 10 × 250 mm). Elution was carried out with a 40−50% linear gradient of acetonitrile (0.1% TFA) over 50 min. Purified triN36e, obtained in 16% yield, was identified by ESI-TOF-MS. The detailed synthesis of peptides is described in the Supporting Information (SI).

CD Spectra. CD measurements were performed with a J-720 circular dichroism spectrolarimeter equipped with a thermoregulator (JASCO). The wavelength dependence of molar ellipticity [θ] was monitored at 25 °C from 190 to 250 nm. Peptides were dissolved in 20 mM acetate buffer (pH 4.0) containing 40% MeOH (*23, 24*). The experimental helicity was calculated as reported previously (*17*−*19*).

Immunization and Sample Collection. Six-week-old male BALB/c mice were purchased from Sankyo Laboratory Service Corp. (Tokyo, Japan) and maintained under specific pathogen-free conditions in an animal facility. The experimental protocol was approved by the ethical review committee of Tokyo Medical and Dental University. Freund incomplete adjuvant and PBS

* To whom correspondence should be addressed. E-mail: nomura.mr@tmd.ac.jp; tamamura.mr@tmd.ac.jp. phone: +81-3-5280-8036, fax: +81-3-5280-8039.

[†] Tokyo Medical and Dental University.

[‡] National Institute of Infectious Diseases.

10.1021/bc900502z
Published on Web 04/01/2010

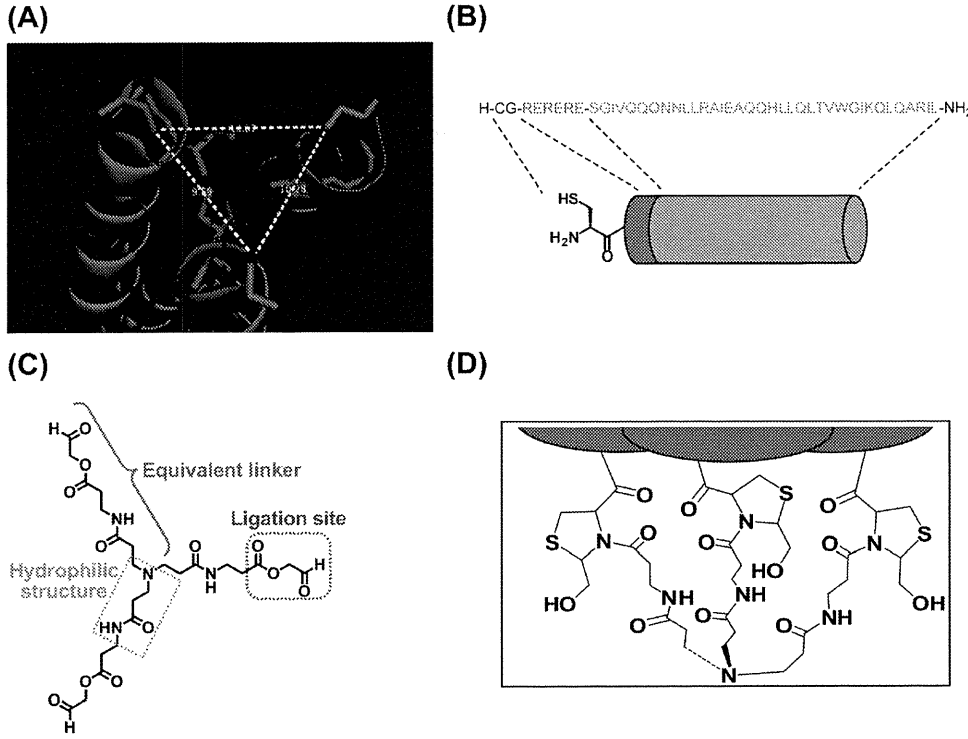

Figure 1. (A) Distances between hydrogen atoms for hydroxyl groups in N-terminal serine residues of N36 helices in trimeric form. The distances were evaluated by PyMOL (*21*). (B) Cartoon presentation of each N36 derived peptide, N36REGC. (C) Design of a C3-symmetric template. The amino acid residues are described in single letters. (D) Conjugated structure of trimeric N36 after thiazolidine ligation.

were purchased from Wako Pure Chemical Industries (Osaka, Japan). DMSO (endotoxin free) was purchased from Sigma-Aldrich (St. Louis, MO).

All mice were bled one week before immunization. One hundred micrograms of antigen was dissolved in 1 μL of DMSO. The solution was mixed with 50 μL of PBS and 50 μL of Freund incomplete adjuvant. The mixture was injected subcutaneously under anesthesia on days 0, 14, 28, 42, and 58. Mice were bled on days 21, 35, 49, and 65. Serum was separated by centrifugation (15 000 rpm) at 4 °C for 15 min and inactivated at 56 °C for 30 min. Sera were stored at −80 °C before use.

Serum Titer ELISA. Tween-20 (polyoxyethylene (20) sorbitan monolaurate) and hydrogen peroxide (30%) were purchased from Wako. ABTS (2,2-azino-bis(3-ethylbenzothiazoline-6-sulfonic acid) diammonium salt) was purchased from Sigma-Aldrich. Antimouse IgG (H+L)(goat)-HRP was purchased from EMD Chemicals (San Diego, CA). Ninty-six-well microplates were coated with 25 μL of a synthetic peptide at 10 μg/mL in PBS at 4 °C for overnight. The coated plates were washed 10 times with deionized water and blocked with 150 μL of blocking buffer (0.02% PBST, PBS with 0.02% Tween 20, containing 5% skim milk) at 37 °C for 1 h. The plates were washed with deionized water 10 times. Mice sera were diluted in 0.02% PBST with 1% skim milk, and 50 μL of 2-fold serial dilutions of sera from 1/200 to 1/102400 were added to the wells and allowed to incubate at 37 °C for 2 h. The plates were washed 10 times with deionized water. Twenty-five microliters of HRP-conjugated antimouse IgG, diluted 1:2000 in 0.02% PBST, was added to each well. After 45 min incubation, the plates were washed 10 times and 25 μL of HRP substrate, prepared by dissolving 10 mg ABTS to 200 μLof HRP staining buffer—a mixture of 0.5 M citrate buffer (pH 4.0, 1 mL), H_2O_2 (3 μL), and H_2O (8.8 mL)—was added. After 30 min incubation, the reaction was stopped by addition of 25 μL/well 0.5 M H_2SO_4, and optical densities were measured at 405 nm.

Virus Preparation. The pNL4-3 construct (8 μg) was transfected into 293T cells by Lipofectamine LTX (Invitrogen, Carlsbad, CA) followed by changing medium at 12 h after transfection. At 48 h after changing medium, the supernatant was collected, passed through a 0.45 μm filter, and stored at −80 °C as HIV-1_{NL4-3} strain before use. For titration, MT-4 cells were infected with serially 3-fold diluted virus from 1/10 to 1/196830, and cultured for 7 days. HIV-1 p24 levels in supernatants were measured, and then the titer of virus solution was calculated.

Anti-HIV Assay. Virus was prepared as described above except that the transfection of pNL4-3 was performed by the calcium phosphate method. Anti-HIV-1 activity was determined on the basis of protection against HIV-1-induced cytopathogenicity in MT-4 cells. Various concentrations of AZT, N36RE, and triN36e (The starting concentrations are 100, 10, and 1 μM, respectively) were added to HIV-1-infected MT-4 cells (MOI = 0.01) by 2-fold serial dilution and placed in wells of a flat-bottomed microtiter plate (2.0×10^4 cells/well). After 5 days' incubation at 37 °C in a CO_2 incubator, the number of viable cells was determined using the 3-(4,5-dimethylthiazol-2-yl)-2,5-diphenyltetrazolium bromide (MTT) method (EC_{50}). Cytotoxicity of compounds was determined on the basis of viability of mock-infected cells using the MTT method (CC_{50}). Each experiment was performed three times independently.

Neutralizing Assay. MT4-cells (1×10^5 cells/100 μL) were incubated in 100 μL medium containing 10 μL sera from immunized or preimmunized mice for 1 h at 37 °C, then pretreated MT-4 cells were infected with HIV-1_{NL4-3} (MOI = 0.05). At 3 days after infection, cells were collected by centrifuge at 4000 rpm for 10 min at 4 °C. After discarding supernatant, pellets were lysed with 30 μL of lysis buffer (50 mM Tris·HCl (pH 7.5), 150 mM NaCl, 1% NP-40), then 30 μL of 2 × SDS buffer (125 mM Tris·HCl (pH 6.8), 4% SDS, 20% glycerol, 10% 2-ME, 0.004% BPB) were added and boiled for 10 min. The samples (5 μL) were subjected to SDS-page to perform Western blotting. The HIV-1 gag p24 was detected by using Western lightning ECL kit (PerkinElmer, MA) according to manufacturer's instruction after treatment of HIV-1 p24